Molecular Origin of Continuous Dark Noise in Rod Photoreceptors

F. Rieke and D. A. Baylor
Department of Neurobiology, Stanford University, Stanford, California 94305 USA

ABSTRACT Noise in the rod photoreceptors limits the ability of the dark-adapted visual system to detect dim lights. We investigated the molecular mechanism of the continuous component of the electrical dark noise in toad rods. Membrane current was recorded from intact, isolated rods or truncated, internally dialyzed rod outer segments. The continuous noise was separated from noise due to thermal activation of rhodopsin and to transitions in the cGMP-activated channels. Selectively disabling different elements of the phototransduction cascade allowed examination of their contributions to the continuous noise. These experiments indicate that the noise is generated by spontaneous activation of cGMP phosphodiesterase (PDE) through a process that does not involve transducin. The addition of recombinant gamma, the inhibitory subunit of PDE, did not suppress the noise, indicating that endogenous gamma does not completely dissociate from the catalytic subunit of PDE during spontaneous activation. Quantitative analysis of the noise provided estimates of the rate constants for spontaneous PDE activation and deactivation and the catalytic activity of a single PDE molecule in situ.

INTRODUCTION

The classic psychophysical experiments of Hecht, Shlaer, and Pirenne (1942) demonstrate that the dark-adapted visual system can successfully detect the absorption of 5–7 photons. More recent work indicates that the ultimate limit on the accuracy of photon counting is imposed by dark noise in the retinal rods. The measured dark noise of single rods (Baylor et al., 1980, 1984) is in good agreement with the noise inferred from retinal ganglion cell recordings (Barlow et al., 1971; Copenhagen et al., 1987; Aho et al., 1993) and psychophysical experiments (Barlow, 1956; Sakitt, 1972; Aho et al., 1988).

In darkness, retinal rods are partially depolarized by an inward current through cationic channels held open by cyclic GMP (cGMP). Light lowers the internal concentration of cGMP, allowing the channels to close and reducing the inward current (reviewed by Lagnado and Baylor, 1992; Yarfitz and Hurley, 1994; Fig. 1). The resulting membrane hyperpolarization modulates transmitter release at the synaptic terminal, allowing the visual message to go forward. Recordings of the membrane current of single rods (Baylor et al., 1980) show two main components of noise in the frequency band that comprises the single-photon response: discrete events resembling responses to single photons, and a continuously present fluctuation with a root-mean-square amplitude about one-fifth that of the photon response. Each component contributes roughly equally to the total variance of the current in darkness. The photon-like component of the dark noise arises from thermal activation of rhodopsin (Baylor et al., 1980); the molecular mechanism of the continuous component is not known.

Previous work has shown that the continuous noise variance scales linearly with the fraction of the outer segment from which the current is recorded (Baylor et al., 1980), indicating that the noise is generated in the outer segment. Furthermore, the noise persists when a rod is voltage-clamped (Bodoia and Detwiler, 1984; Gray and Attwell, 1985), indicating that the noise arises from fluctuations in outer-segment conductance rather than fluctuations in the driving potential on the outer-segment current. The frequency composition of the continuous noise can be predicted from the kinetics of the cell's response to a dim flash (Baylor et al., 1980). This behavior suggests that the noise arises in the transduction cascade downstream from rhodopsin. Regardless of the source, the noise must ultimately be produced by gating or blocking transitions in the cGMP-activated channels. If the probabilities for transitions between channel states are stationary, the noise should have a power spectrum consisting of a sum of Lorentzians (Colquhoun and Hawkes, 1977). The spectrum observed—a product of Lorentzians—suggests instead that the noise involves changes in the transition probabilities between channel states, as would result from fluctuations in the internal concentration of cGMP.

We evaluated the contributions of two potential sources for fluctuations in the cGMP concentration: variations in the rate of cGMP synthesis (Rispoli et al., 1991), which is catalyzed by guanylate cyclase, and variations in the rate of cGMP hydrolysis (Lamb, 1987; Leibrock et al., 1994), which is catalyzed by cGMP phosphodiesterase (PDE). We show that the continuous noise arises from fluctuations in PDE activity and examine the molecular basis for these fluctuations as well as their impact on the function of the transduction cascade.

Received for publication 12 June 1996 and in final form 7 August 1996.

Address reprint requests to Dr. Fred Rieke, Department of Neurobiology, Stanford University, Stanford, CA 94305. Tel.: 415-723-7556; Fax: 415-725-3958; E-mail: rieke@leland.stanford.edu.

0006-3495/96/11/2553/20 $2.00

MATERIALS AND METHODS

Preparations and electrical recording

Experiments were performed on rod photoreceptors from the retina of the toad *Bufo marinus*. All animal procedures conformed with protocols ap-

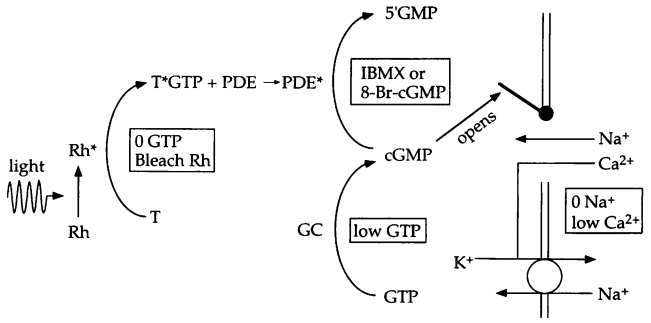

FIGURE 1 Schematic diagram of phototransduction cascade. Current flows into the outer segment in darkness through channels held open by cGMP. The cGMP concentration in the outer segment, and thus the number of open channels, reflects a balance between the rate of cGMP synthesis by guanylate cyclase (GC) and the rate of hydrolysis by phosphodiesterase (PDE). Light closes membrane channels by lowering the cGMP concentration: photoexcited rhodopsin activates a G-protein, transducin (T), which in turn activates the PDE. During the light response the Ca^{2+} concentration in the outer segment decreases as Ca^{2+} influx through the channels slows, while Ca^{2+} efflux by Na^+/K^+, Ca^{2+} exchange continues. The light-induced fall in Ca^{2+} regulates several elements of the cascade to oppose changes in current. Our experimental strategy was to disable different elements of the transduction cascade while observing the effect on the continuous noise. The manipulations used to disable parts of the cascade (boxes) are described in Materials and Methods.

proved by the Administrative Panel on Laboratory Animal Care at Stanford University. Toads were dark-adapted 12–15 h, rapidly decapitated and pithed, and the eyes removed. These initial steps were carried out under dim red light; all subsequent steps were carried out under infrared illumination using a dissecting microscope equipped with infrared/visible image converters. The posterior half of each eye was cut into four pieces and transferred to a petri dish containing Ringer's, where the retina was gently peeled from the pigment epithelium. Isolated pieces of retina were stored for up to 36 h in Ringer's at 4°C. Isolated rods were obtained by shredding a small piece of retina (roughly 2 mm^2) with fine needles in a 100-μl drop of Ringer's. The drop was then injected into a recording chamber mounted on the stage of an inverted microscope (Zeiss Axiovert) equipped with an infrared video viewing system.

An isolated rod was drawn by suction into a heat-polished, silanized borosilicate electrode with an opening 5–6 μm in diameter. For truncation experiments (Yau and Nakatani, 1985), the outer segment was drawn into the electrode and the inner segment, together with the base of the outer segment was cut off with a sharp probe, allowing diffusional access to the cytoplasm of the outer segment. For Ca^{2+} clamp experiments on intact rods (Nakatani and Yau, 1988b; Matthews et al., 1988), the inner segment was drawn into the electrode so that the solution bathing the outer segment could be rapidly changed.

Electrical connections to the bath and suction electrode were made by Ringer's-filled agar bridges that contacted calomel half-cells. Bath voltage was held at ground by an active clamp circuit (Baylor et al., 1984). During experiments on truncated outer segments, the electrode and bath were maintained at the same voltage, so that the potential difference across the outer segment membrane was zero. During Ca^{2+} clamp experiments on intact cells, the voltage between the electrode and bath was adjusted to offset a 0.3–0.5-mV junction potential introduced when the outer segment was exposed to Na^+-free solution (see Table 1). In both types of experiment, membrane current collected by the suction electrode was amplified by an Axopatch 200A patch-clamp amplifier (Axon Instruments, Foster City, CA), filtered at 20 Hz (−3 dB point) with an 8-pole Bessel low-pass filter, and digitized at 100 Hz.

The one-sided power spectral density of the current $I(t)$ is given by

$$S(\omega) = \frac{2\langle|\tilde{I}(\omega)|^2\rangle}{T}, \quad (1)$$

where $\tilde{I}(\omega) = \int_0^T dt\, I(t) \exp(i\omega t)$ is the Fourier transform of $I(t)$, ω is the temporal frequency in radians s^{-1}, and the average $\langle\cdots\rangle$ is over repeated measurements of the current during time intervals of length T. Noise power spectra were computed according to Eq. 1 from continuous stretches of record 20.48 s long. Before the power spectrum was calculated, linear trends were removed by subtracting the best-fitting straight line from each 20.48-s recording. At frequencies above 1 Hz, power spectra were smoothed by averaging over five neighboring points. Power spectra were calculated from interleaved stretches of record when the noise was measured in the same cell under different conditions. For measurement of channel noise the membrane current was filtered at 3 kHz (−3 dB point) and digitized at 10 kHz. Power spectra were computed from 1.6384-s stretches of record without linear trend removal and smoothed by averaging over five points between 0 and 60 Hz, 20 points between 60 and 300 Hz, and 100 points between 300 and 2000 Hz. During noise measurements all light paths into the Faraday cage were sealed.

Compositions of the internal and external solutions are listed in Table 1. Free Ca^{2+} concentrations were measured with a Ca^{2+} electrode (Orion Instruments, Boston, MA). Cyclic GMP concentrations measured spectroscopically were found to be systematically 10% lower than expected from the molecular weight, presumably from an increase in water content during storage. During truncation experiments, the Ca^{2+} concentration in the outer

TABLE 1 Concentrations (in mM) of the constituents of each solution

	Ringer's	Truncation dialysis	Truncation electrode	Ca^{2+} clamp
NaCl (mM)	120	—	120	—
KCl	2	—	—	—
$NaHCO_3$	2	—	—	—
$CaCl_2$	1	0.75	0.05	0.25
$MgCl_2$	1.6	1.6	1.6	—
Glucose	10	—	—	—
HEPES	3	3	3	3
EGTA	—	—	1	1
BAPTA	—	1	—	—
Arginine-glutamate	—	120	—	—
Choline-Cl	—	—	—	120

The pH of all solutions was 7.6. In the truncation dialysis and Ca^{2+} clamp solutions the pH was adjusted with TMA-OH, and in other solutions it was adjusted with NaOH. Osmolarity was 245 mOsm in the truncation dialysis solution and 260 mOsm in all others. The free Ca^{2+} concentration in the truncation dialysis solution was measured with a Ca^{2+} electrode as 500–600 nM. The free Ca^{2+} concentration in the Ca^{2+} clamp solution was calculated as approximately 10 nM.

segment was held constant by buffering the Ca^{2+} in the dialyzing solution with 1 mM (1,2-bis(2-aminophenoxy)-ethane-*N,N,N',N'*-tetraacetic acid) (BAPTA) and omitting K^+ from internal and external solutions to disable Na^+/K^+, Ca^{2+} exchange; the measured free Ca^{2+} concentration in the dialyzing solution was 500–600 nM. Under these conditions the dark current was carried mainly by inward movement of Na^+. During Ca^{2+} clamp experiments on intact cells, the inner segment was drawn into the suction electrode, which contained Ringer's. The Ca^{2+} concentration in the outer segment was held constant by bathing it in a solution that blocked Ca^{2+} efflux and minimized influx. This was accomplished by replacing external Na^+ with choline to disable Na^+/K^+, Ca^{2+} exchange and buffering external Ca^{2+} to a concentration of 10 nM. This concentration was chosen to null the electrochemical driving force on Ca^{2+}, assuming an internal Ca^{2+} concentration of 500 nM in darkness (Gray-Keller and Detwiler, 1994; McCarthy et al., 1994) and a membrane potential of −50 mV. The effectiveness of the Ca^{2+} clamp was tested by measuring dim flash responses with the Ca^{2+} clamped before and after increasing the outer segment's Ca^{2+} buffering capacity by perfusing with BAPTA-AM. Additional Ca^{2+} buffering did not change the kinetics of the flash response with the Ca^{2+} clamped, indicating that residual changes in Ca^{2+} were small. With the Ca^{2+} clamped the dark current was carried mainly by outward movement of K^+; as a result the light responses had a polarity opposite those measured in Ringer's.

The composition of the solution bathing the outer segment of an intact cell or the cut end of a truncated outer segment was changed by switching a flowing solution driven by positive pressure from a tapered glass delivery pipe with an opening 100–200 μm in diameter. Solution entered the delivery pipe from one of several 200-μm-diameter fused-silica tubes (Polymicro Technologies, Phoenix, AZ) glued into its shank; each tube was connected to a separate electrically controlled pinch valve (Biochem Valves, Boonton, NJ) and pressurized solution reservoir. The solution emerging from the delivery pipe changed in 200–300 ms upon switching valves.

Manipulation of transduction cascade

Elements of the transduction cascade in truncated rod outer segments were selectively disabled by manipulation of nucleotide concentrations and introduction of pharmacological agents (see Fig. 1). These manipulations isolated fluctuations in the transduction current caused by gating transitions in channels at constant cGMP, by fluctuations in the rate of cGMP synthesis, and by fluctuations in the rate of cGMP hydrolysis.

Noise from cGMP-activated channels at a constant internal cGMP concentration was isolated by suppressing cGMP synthesis and hydrolysis. Cyclic GMP synthesis was disabled by removing the precursor, GTP, from the solution dialyzing a truncated outer segment. Cyclic GMP was added to the dialyzing solution to open channels and produce a current. Cyclic GMP hydrolysis was disabled by adding 500 μM isobutyl methylxanthine (IBMX) to the dialyzing solution or by replacing cGMP with 8-bromo-cGMP, an analog that efficiently opens the channel but is hydrolyzed approximately 500 times more slowly than cGMP (Zimmerman et al., 1985). Both IBMX and 8-bromo-cGMP reduced the flash sensitivity of truncated outer segments more than 100-fold, as expected for nearly complete block of hydrolysis. Without synthesis or hydrolysis, the cGMP concentration in the outer segment was simply equal to that in the dialyzing solution.

Noise due to cGMP synthesis was isolated by selectively disabling cGMP hydrolysis with IBMX and providing sufficient GTP to support synthesis. Thus when truncated outer segments were dialyzed with IBMX, GTP, and no cGMP, the upper limb of the transduction cascade in Fig. 1 was disabled and the cGMP concentration was determined by synthesis and diffusion out of the cut end of the outer segment.

Noise due to cGMP hydrolysis was isolated by lowering the GTP concentration in the dialyzing solution to 10 μM, which supported transducin activation but allowed minimal synthesis of cGMP (Lagnado and Baylor, 1994). Evidence for negligible synthesis at 10 μM GTP was obtained by measuring the change in dark current that occurred when the cyclase was strongly activated by low Ca^{2+} (Fig. 2). To make the dark current more sensitive to cGMP synthesis, hydrolysis was inhibited with IBMX. At low Ca^{2+}, cyclase activity is stimulated by a Ca^{2+}-binding protein (reviewed by Koutalos and Yau, 1996); stimulation is half-maximum at about 100 nM Ca^{2+} and has a cooperativity of 2–4 (Koch and Stryer, 1988; Koutalos et al., 1995a). With 200 μM GTP in the dialyzing solution, lowering the Ca^{2+} concentration from 500 to 10 nM increased the dark current, as expected from increased cGMP synthesis (Fig. 2, thick trace). At 10 μM GTP, the same change in Ca^{2+} did not change the dark current (Fig. 2, thin traces). Low Ca^{2+} failed to elicit a change in current at 10 μM GTP in eight experiments. Thus with 10 μM GTP in the dialyzing solution, the lower limb of the transduction cascade in Fig. 1 is disabled, and the cGMP concentration is determined by the rate of cGMP diffusion into the outer segment from the bath and the rate of cGMP hydrolysis.

THEORY

Experiments described in Results indicate that the continuous component of the rod dark noise results from spontaneous activation of PDE. This section presents a quantitative model that relates the measured current fluctuations to PDE activity. First, we describe a kinetic model of fluctuations in PDE activity. Second, we consider how fluctuations in PDE activity affect the cGMP concentration. Third, we consider how changes in the cGMP concentration affect the membrane current. These calculations result in three expressions (Eqs. 15, 18, and 26) that relate the measured noise spectra to the catalytic activity and activation-deactivation kinetics of single PDE molecules under three different experimental conditions. Fitting the measured noise

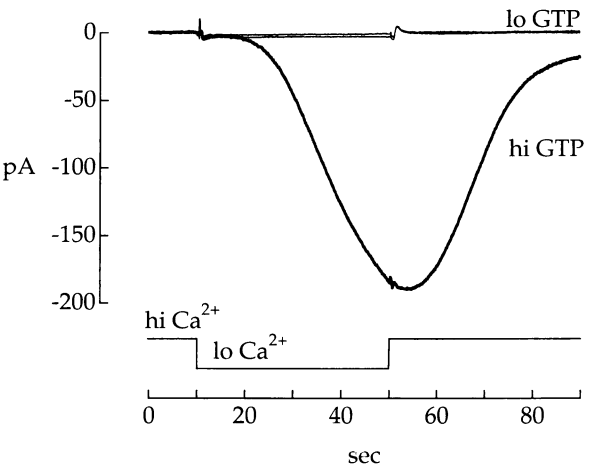

FIGURE 2 Evidence that cGMP synthesis was negligible at low GTP concentration. A truncated outer segment was dialyzed with a solution containing 500 μM IBMX to inhibit cGMP hydrolysis and 200 μM or 10 μM GTP. Cyclic GMP synthesis at the two GTP concentrations was monitored by observing the change in membrane current that occurred when the internal Ca^{2+} concentration was lowered from 500 to 10 nM for the 40-s period indicated. This drop in Ca^{2+} should increase guanylate cyclase activity at least 20-fold (Koch and Stryer, 1988; Koutalos et al., 1995a). As expected, the inward current increased substantially when the Ca^{2+} concentration was lowered in the presence of 200 μM GTP (thick trace). The superposed thin traces at 10 μM GTP were recorded before and after the record at 200 μM GTP; lowering the Ca^{2+} in the presence of this reduced GTP concentration did not produce an obvious change in current.

spectra with Eq. 15, 18, or 26 provided estimates of the catalytic activity and rate constants for activation and deactivation of a single PDE molecule.

Kinetics of PDE fluctuations

We assume that 1) a single PDE molecule can exist in either of two states, active or inactive; 2) the active state is improbable; 3) individual molecules behave independently and have additive catalytic activities. With these assumptions, activation of single PDE molecules is described by Poisson statistics, and the mean and variance of the total PDE activity are given by Campbell's theorem (Rice, 1954). The probability that a given molecule is active is k_1/k_2, where k_1 is the rate constant for spontaneous activation and k_2 is the rate constant for deactivation. The mean spontaneous activity, P_D, of N molecules is

$$P_D = \frac{Nk_1\hat{a}}{k_2}, \tag{2}$$

where $\hat{a}$ is the fractional reduction in the cGMP concentration in the outer segment per unit time produced by a single active PDE catalytic subunit, referred to hereafter as the catalytic activity. The variance of the spontaneous PDE activity is

$$\sigma_P^2 = \frac{Nk_1\hat{a}^2}{k_2}, \tag{3}$$

and the power spectral density of the activity is described by the Lorentzian

$$S_P(\omega) = \frac{4Nk_1\hat{a}^2}{k_2^2 + \omega^2} = \frac{4k_2P_D\hat{a}}{k_2^2 + \omega^2}, \tag{4}$$

where the angular frequency in radians s^{-1}, ω, is related to the frequency f in Hz by $\omega = 2\pi f$.

Kinetics of cGMP concentration changes

The fluctuations in PDE activity described in Eqs. 2–4 cause fluctuations in the cGMP concentration. The dependence of cGMP fluctuations on PDE fluctuations is determined by the cGMP concentration, the rate of cGMP synthesis, and the diffusion of cGMP. For cGMP concentrations well below the effective affinity $K_M \approx 0.1$–0.5 mM of the PDE for cGMP (Pugh and Lamb, 1993; Dumke et al., 1994), the hydrolysis rate is PG, where P is the PDE activity and G is the cGMP concentration. Assuming that the outer segment can be treated as a uniform cylinder, we need only consider longitudinal diffusion; in this case the cGMP concentration $G(x, t)$ at time t and position x along the outer segment is described by

$$\frac{\partial G(x,t)}{\partial t} = D\frac{\partial^2 G(x,t)}{\partial x^2} - P(x,t)G(x,t) + \gamma, \tag{5}$$

where D is the effective longitudinal diffusion coefficient for cGMP and γ is the rate of cGMP synthesis. The first term on the right describes the net diffusional flux of cGMP at position x created by positional variation in the cGMP concentration. The second and third terms account for hydrolysis and synthesis of cGMP. The solution to Eq. 5 under a given set of experimental conditions determines the relation between fluctuations in PDE activity and fluctuations in cGMP concentration.

Relation between current fluctuations and cGMP concentration changes

When the cGMP concentration along the outer segment is spatially uniform, the dependence of the current on cGMP concentration can be approximated as $I \approx hG^3$ (see Fig. 12 *A* and Eqs. 27 and 28), where h is a constant that depends on the maximum current and the affinity of the channel for cGMP (see Eq. 28); the approximation is valid when the current is well below the maximum current produced by saturating cGMP. A small change δG in the cGMP concentration produces a change in current given by

$$\delta I \approx \frac{dI}{dG}\delta G \approx 3hG^2\delta G. \tag{6}$$

In the presence of spatial fluctuations or gradients in the cGMP concentration, the measured current can be expressed as $I_{meas} = \int_0^L dx\ \phi(x)$, where L is the outer segment length and $\phi(x)\,dx = hG^3(x)\,dx/L$ is the current between x and $x + dx$ produced by a cGMP concentration $G(x)$. A fluctuation $\delta G(x)$ in the cGMP concentration produces a change in current density $\delta\phi(x)$ at position x described by

$$\delta\phi(x) \approx \frac{\partial\phi(x)}{\partial G(x)}\delta G(x) \approx 3hG^2(x)\delta G(x)/L, \tag{7}$$

and a change $\delta I_{meas} = \int_0^L dx\ \delta\phi(x)$ in the measured current.

Equations 4, 5, and 7 determine the relation between fluctuations in PDE activity and membrane current. Solving Eq. 5 for a given set of experimental conditions allows one to predict the spectrum of membrane current fluctuations.

Truncated outer segments without cGMP synthesis

In the absence of cGMP synthesis (when $\gamma = 0$), the steady-state concentration profile of cGMP and the fluctuations about the steady state are determined by diffusion and hydrolysis. The (time- and position-dependent) cGMP con-

centration can be determined by solving Eq. 5 subject to the requirements that 1) the cGMP concentration at the cut end of the outer segment is equal to that in the dialyzing solution and 2) the flux of cGMP at the uncut end of the outer segment is zero. These requirements are expressed by the boundary conditions

$$G(L, t) = G_0$$
$$\left.\frac{\partial G}{\partial x}\right|_{x=0} = 0, \tag{8}$$

where G_0 is the cGMP concentration in the dialyzing solution and L is the outer segment length. The cut end of the outer segment is taken to be at $x = L$ and the tip at $x = 0$.

Hydrolysis causes the cGMP concentration to fall with distance from the cut end of the outer segment, and this gradient causes a steady diffusional flux of cGMP into the outer segment from the bath. The steady-state solution of Eq. 5 subject to the boundary conditions in Eq. 8 is

$$G_{ss}(x) = G_0\frac{\cosh(x/\lambda)}{\cosh(L/\lambda)}, \tag{9}$$

where $\lambda = \sqrt{D/P_D}$, D is the longitudinal diffusion coefficient for cGMP, and P_D is the mean dark PDE activity; λ is a length constant that specifies the decline in cGMP concentration with distance from the cut end.

How does a fluctuation $\delta P(t)$ in the PDE activity at position x_0 along the outer segment affect the cGMP concentration and in turn the current? $\delta P(t)$ produces a change $\delta G(x, t; x_0)$ in the cGMP concentration. $\delta G(x, t; x_0)$ denotes the change in cGMP concentration at position x and time t produced by the PDE fluctuation at position x_0. The total cGMP concentration is $G(x; t) = G_{ss}(x) + \delta G(x, t; x_0)$, and the total PDE activity is $P(x, t) = P_D + \delta P(t)$. When these expressions are used to replace G and P in Eq. 5, the term $\delta G\delta P$ can be dropped, provided δG and δP are small. The resulting equation for δG is

$$\frac{\partial}{\partial t}\delta G(x, t; x_0)$$
$$= D\frac{\partial^2}{\partial x^2}\delta G(x, t; x_0) - \delta P(t)G_{ss}(x) - P_D\delta G(x, t; x_0). \tag{10}$$

Equation 10 determines how the cGMP concentration fluctuates about the steady-state level $G_{ss}(x)$. The boundary conditions for $\delta G(x, t;x_0)$ are given by Eq. 8 with $\delta G_0(L, t; x_0) = 0$ to ensure that the total cGMP concentration at the cut end is G_0. Solving Eq. 10 using Fourier techniques (see, for example, Carslaw and Jaeger, 1959) yields an expression for the change in cGMP:

$$\delta\tilde{G}(x, \omega; x_0) =$$
$$-\frac{2\delta\tilde{P}(\omega)G_0\cosh(x_0/\lambda)}{\cosh(L/\lambda)}\sum_n\frac{\cos(x_0/\lambda_n)\cos(x/\lambda_n)}{D/\lambda_n^2 + P_D - i\omega}, \tag{11}$$

where $\lambda_n = 2L(2n + 1)^{-1}\pi^{-1}$, and the Fourier transform of a function $f(t)$ is defined as $\tilde{f}(\omega) = \int dt\, \exp(i\omega t)\, f(t)$.

The change in current density $\delta\tilde{\phi}(x,\omega; x_0)$ at position x and frequency ω produced by the fluctuation $\delta\tilde{G}(x, \omega; x_0)$ is given by Eq. 7 with $G(x) = G_{ss}(x)$. Substituting for G_{ss} and δG from Eqs. 9 and 11, we obtain

$$\delta\tilde{\phi}(x, \omega; x_0)$$
$$= \frac{6\delta\tilde{P}(\omega)hG_0^3\cosh^2(x/\lambda)\cosh(x_0/\lambda)}{L\cosh^3(L/\lambda)}\sum_n\frac{\cos(x_0/\lambda_n)\cos(x/\lambda_n)}{D/\lambda_n^2 + P_D - i\omega}. \tag{12}$$

Equation 12 describes the change in current density at position x and temporal frequency ω produced by a fluctuation $\delta\tilde{P}(\omega)$ in the PDE activity at position x_0. The total change in current $\delta\tilde{I}(\omega; x_0)$ produced by this PDE fluctuation is obtained by integrating Eq. 12 over the length of the outer segment:

$$\delta\tilde{I}(\omega; x_0) = \int_0^L dx\delta\tilde{\phi}(x, \omega; x_0). \tag{13}$$

Equations 12 and 13 give the change in current produced by a fluctuation in PDE activity. To obtain the current noise spectrum, we assume that the PDE fluctuations have a constant longitudinal density and that PDE fluctuations at different locations along the outer segment make independent, additive contributions to the noise (see Baylor et al., 1980). With these assumptions the power spectrum of the current fluctuations is found by averaging $|\delta\tilde{I}(\omega; x_0)|^2$ over the site x_0 of the PDE fluctuation:

$$S_I(\omega) = \left\langle\left|\int_0^L dx\delta\tilde{\phi}(x, \omega; x_0)\right|^2\right\rangle, \tag{14}$$

where $\langle\cdot\cdot\cdot\rangle$ denotes the average over x_0. Using Eqs. 4 and 12, we obtain the noise power spectrum,

$$\frac{S_I(\omega)}{I^2} = \frac{144P_Dk_2\hat{a}}{L(k_2^2 + \omega^2)(\int_0^L dx\cosh^3(x/\lambda))^2}\times$$
$$\int_0^L dx_0\left|\sum_n\frac{\cosh(x_0/\lambda)\cos(x_0/\lambda_n)\int_0^L dx\cosh^2(x/\lambda)\cos(x/\lambda_n)}{D/\lambda_n^2 + P_D - i\omega}\right|^2, \tag{15}$$

where $\phi_{ss}(x) = hG_{ss}^3(x)/L$, and $\langle|\delta\tilde{P}(\omega)|^2\rangle$ has been replaced with $S_P(\omega)$ from Eq. 4. The power spectrum in Eq. 15 has been normalized by the square of the dark current to facilitate comparison of measured noise spectra in different experiments. The shape of the noise spectrum is determined by the deactivation time $1/k_2$ for PDE (first term on the right side of Eq. 15) and the time required to replenish the cGMP hydrolyzed by the active PDE (second term in Eq. 15). If each of these processes on average had an exponential time

dependence, the spectrum would take the form of a product of two Lorentzians:

$$S(\omega) \propto \frac{1}{(1 + \omega^2/k_2^2)} \frac{1}{(1 + \omega^2/k_{cGMP}^2)}, \quad (16)$$

where k_{cGMP} is the rate constant for cGMP replenishment. In the truncated outer segment, however, cGMP replenishment does not follow a simple exponential time course, and the expected noise spectrum is described by Eq. 15.

The predicted shape of the continuous noise spectrum in Eq. 15 depends on five parameters: the effective longitudinal diffusion coefficient for cGMP D, the mean dark PDE activity P_D, the outer segment length L, the rate constant k_2 for PDE deactivation, and the catalytic activity $\hat{a}$ of a single active PDE molecule. Independent measurement of D, P_D, and L (see Results) allowed k_2 and $\hat{a}$ to be estimated by fitting Eq. 15 to the measured noise spectra in truncated outer segments in which cGMP synthesis was disabled.

Truncated outer segments with cGMP synthesis

In a truncated outer segment dialyzed with high GTP and no cGMP, the cGMP concentration in the outer segment is determined by synthesis, hydrolysis, and diffusion out of the cut end. We assume that the synthesis rate along the outer segment is uniform, which should be the case in outer segments dialyzed with high concentrations of GTP so that the substrate for synthesis is plentiful throughout. This situation is described by Eq. 5 subject to the boundary conditions in Eq. 8 with $G_0 = 0$. The steady-state cGMP concentration is

$$G_{ss}(x) = \frac{\gamma}{P_D}\left[1 - \frac{\cosh(x/\lambda)}{\cosh(L/\lambda)}\right], \quad (17)$$

where γ is the rate of cGMP synthesis, $\lambda = \sqrt{D/P_D}$, D is the longitudinal diffusion coefficient for cGMP, and P_D is the mean dark PDE activity. The change in cGMP concentration produced by a fluctuation δP in the PDE activity at position x_0 is again described by Eq. 11. An expression for the shape of the noise spectrum is obtained from arguments similar to those used in obtaining Eqs. 12–15. The spectrum takes the form

$$\frac{S_I(\omega)}{I^2} = \frac{144 P_D k_2 \hat{a}}{L(k_2^2 + \omega^2)(\int dx g^3(x))^2} \times \int dx_0 \left| \sum_n \frac{g(x_0)\cos(x_0/\lambda_n)\int dx g^2(x)\cos(x/\lambda_n)}{D/\lambda_n^2 + P_D - i\omega} \right|^2, \quad (18)$$

where $g(x) = \cosh(L/\lambda) - \cosh(x/\lambda)$. Again, the shape of the calculated noise spectrum is determined by the deactivation rate constant of PDE and the time required to replenish the hydrolyzed cGMP. Equation 18, in conjunction with independent measurement of P_D, D, and L, allowed estimates to be made of the deactivation rate constant k_2 and catalytic activity $\hat{a}$ from noise spectra measured in truncated cells with cGMP synthesis active.

Intact rods

In intact rods, unlike truncated outer segments, the average cGMP concentration is spatially uniform, and there is no net diffusional flux of cGMP into or out of the outer segment. Diffusion does, however, influence the spatial extent of the cGMP concentration change produced by a localized fluctuation in PDE activity. Provided the current change is linearly related to the fluctuation in PDE activity, the total change in current depends only on the total change in cGMP and not its spatial extent. Thus Eq. 5 can be simplified to

$$\frac{dG}{dt} = \gamma - PG, \quad (19)$$

where γ is the rate of cGMP synthesis, P is the PDE activity, and G is the cGMP concentration.

Ca^{2+} feedback opposes changes in the transduction current in several ways (reviewed by Koutalos and Yau, 1996). Here we consider only the Ca^{2+} dependence of the rate of cGMP synthesis, which is expected to dominate at Ca^{2+} concentrations near the dark level (Koutalos et al., 1995c). We describe the Ca^{2+} dependence of the synthesis rate by (Koch and Stryer, 1988; Koutalos et al., 1995a)

$$\gamma = \frac{\gamma_{max}}{1 + (C/K_{GC})^2} \approx \alpha C^{-2}, \quad (20)$$

where C is the Ca^{2+} concentration, $K_{GC} \approx 100$ nM is the Ca^{2+} concentration at which the cyclase is half-activated, and $\alpha = \gamma_{max} K_{GC}^2$. The approximation is valid when $C \gg K_{GC}$.

The Ca^{2+} concentration is controlled by influx through the channels and extrusion by $Na^+/K^+,Ca^{2+}$ exchange (Cervetto et al., 1989). Complete description of the exchange current kinetics requires at least two time constants (Rispoli et al., 1993; Gray-Keller and Detwiler, 1994; McCarthy et al., 1996; Fig. 13). For temporal frequencies above 0.1 Hz, the fastest time constant dominates and the kinetic operation of the exchanger can be approximated with a single rate constant β. In this case the Ca^{2+} concentration is determined by Ca^{2+} influx through the channels, which comprises a constant fraction of the total inward current (Nakatani and Yau, 1988c), and Ca^{2+} efflux:

$$\frac{dC}{dt} = qhG^3 - \beta C, \quad (21)$$

where q is a constant that relates the membrane current to changes in free Ca^{2+}; thus q depends on the fraction of the current carried by Ca^{2+}, the outer segment volume, and the fraction of Ca^{2+} buffered.

The change in cGMP produced by a small perturbation δP in PDE activity can be estimated assuming that the

changes in the cGMP concentration, δG, and changes in Ca^{2+} concentration, δC, are small. In this case, Eqs. 19 and 21 can be approximated by the linear differential equations

$$\frac{d(\delta G)}{dt} = -\frac{2G_D P_D}{C_D}\delta C - G_D \delta P - P_D \delta G \qquad (22)$$

and

$$\frac{d(\delta C)}{dt} = \frac{3\beta C_D}{G_D}\delta G - \beta \delta C, \qquad (23)$$

in which we have used the steady-state relations $G_D P_D = \alpha/C_D^2$ and $qhG_D^3 = \beta C_D$ between the dark cGMP concentration G_D, PDE activity P_D, and Ca^{2+} concentration C_D. Solving these coupled linear differential equations by Fourier techniques yields an expression for the change in cGMP concentration, δG, produced by a change in PDE activity, δP:

$$\delta\tilde{G}(\omega) = \tilde{F}(\omega)\delta\tilde{P}(\omega), \qquad (24)$$

where the filter F relating changes in PDE activity to changes in cGMP concentration is given by

$$\tilde{F}(\omega) = -G_D\left[P_D + \frac{6\beta^2 P_D}{\beta^2+\omega^2} - i\omega + \frac{6i\omega\beta P_D}{\beta^2+\omega^2}\right]^{-1}. \qquad (25)$$

From Eq. 6, the current change δI produced by a small fluctuation δG in the cGMP concentration is $\delta I/I = 3\,\delta G/G$. This expression for the current fluctuation and Eqs. 4 and 24 predict the form of the current noise spectrum as

$$\frac{S_I(\omega)}{I^2} = \frac{36\hat{a}k_2 P_D}{(k_2^2+\omega^2)\left[P_D^2\left(1+\frac{6\beta^2}{\beta^2+\omega^2}\right)^2 + \omega^2\left(1-\frac{6P_D\beta}{\beta^2+\omega^2}\right)^2\right]}. \qquad (26)$$

As before, the shape of the spectrum is determined by the rate constant for PDE deactivation (first term in the denominator) and the kinetics of replenishment of hydrolyzed cGMP (second term in the denomimator).

The continuous noise spectrum in intact toad rods has previously been fitted by a product of two Lorentzians with equal half-power frequencies (Baylor et al., 1980). Equation 26 is considerably closer to a product of two Lorentzians than a single Lorentzian or a product of three. The spectrum in Eq. 26 falls off slightly more quickly than a product of two Lorentzians and is somewhat flatter at low frequencies, but these differences are difficult to resolve experimentally.

RESULTS

Isolation of continuous noise

Noise in the dark current of rod photoreceptors consists of three known components: 1) discrete events arising from thermal activation of rhodopsin (Baylor et al., 1980), 2) continuous noise arising within the phototransduction cascade (Baylor et al., 1980), and 3) fluctuations arising from gating and/or blocking transitions in the cGMP-activated channels (Bodoia and Detwiler, 1984; Gray and Attwell, 1985; Matthews, 1986). All three components were present in experiments on truncated rod outer segments dialyzed with ATP (which allowed shutoff of photoexcited rhodopsin) and GTP (which allowed synthesis of cGMP and activation of transducin). The power spectrum of the continuous noise was obtained in isolation from the other components by removing from the total dark noise the noise due to thermal activation of rhodopsin and that due to transitions in the cGMP-activated channels.

Removal of discrete noise

Fig. 3 *A* illustrates membrane current recorded from a truncated outer segment in darkness (above) and saturating light (below). Discrete events due to thermal activation of rhodopsin are marked by arrows; for comparison the average dim flash response is shown above the dark records. Power spectra of current fluctuations recorded from the outer segment in darkness and in saturating light are shown in Fig. 3 *B*. To remove the component of noise arising from spontaneous activation of rhodopsin, discrete events were identified and sections of record containing them were removed before the dark spectrum was computed. The spectrum in saturating light isolates instrumental noise, as all the channels in the outer segment are closed and the membrane current is zero (Baylor et al., 1979a; Baylor and Nunn, 1986). The Johnson noise level calculated for the measured leakage conductance between the wall of the suction electrode and the membrane was 1.3×10^{-3} pA^2/Hz in the experiment of Fig. 3 *B*. At frequencies below 1 Hz, excess instrumental noise is apparent. Assuming that the instrumental noise and cellular noise are independent and additive, the spectrum of the cell's dark noise can be obtained as the difference spectrum (dark − light). This difference spectrum, shown in Fig. 3 *C*, should not contain a component arising from thermal activation of rhodopsin, because records containing discrete events were excluded when the raw spectrum was computed.

Two observations indicate that the procedure described above successfully removed noise attributable to the thermal activation of rhodopsin. First, the shape of the noise spectrum differed significantly from the power spectrum of the cell's dim flash response (Fig. 3 *C*, open triangles and inset). Second, the probability density of the current fluctuation amplitudes was symmetrical (Fig. 3 *D*). Discrete events due to thermal activation of rhodopsin produce a bump on the right side of the amplitude distribution because they are monophasic and positive going (Baylor et al., 1980). The Gaussian shape of the distribution indicates that the low-frequency noise is composed of small unitary events occurring at relatively high frequency. In all subsequent spectra, the component of noise arising from sponta-

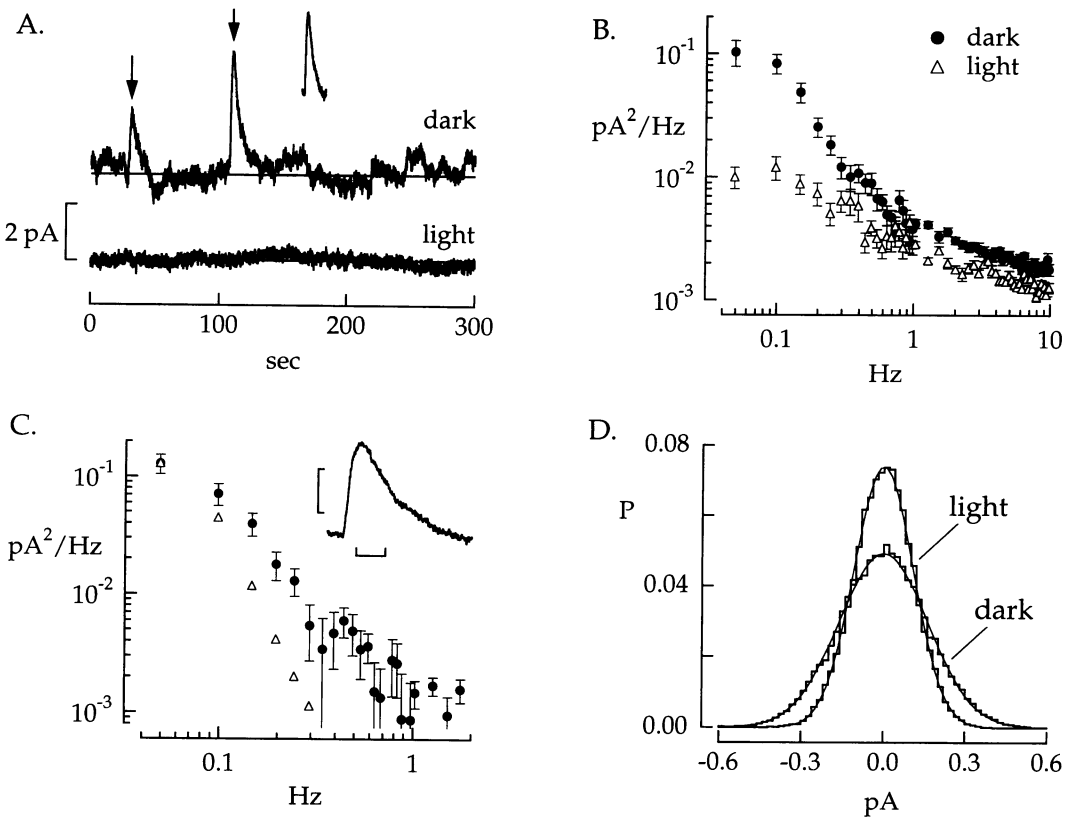

FIGURE 3 Separation of continuous component of dark noise from discrete component. (*A*) Records of a truncated outer segment's membrane current in darkness and saturating light. Two discrete events, resembling responses to single photons, are marked by arrows; the form of the outer segment's average dim flash response is shown in the inset. (*B*) Power spectra of the current noise in darkness computed from records lacking discrete events (●) and records in saturating light (△). The light spectrum measures instrumental noise. At frequencies above 1 Hz the dark spectrum lies slightly above the light spectrum due to channel noise. At frequencies below 1 Hz, the dark spectrum is well above the light spectrum due to the continuous component of the dark noise. Spectra (mean ± SEM) computed from 25 records, each 20.48 s long, low-pass filtered at 20 Hz and sampled at 100 Hz. (*C*) Difference spectrum (dark − light) from *B* (●) compared with the spectrum of the outer segment's dim flash response (△). The flash response spectrum has been scaled vertically to make it coincide with the noise spectrum at 0.05 Hz. The average response to a flash delivering 1.2 photons μm^{-2} at 500 nm is shown in the inset; the vertical scale bar is 2 pA, the horizontal scale bar 4 s. (*D*) Amplitude density of current fluctuations in darkness and saturating light. Dark amplitudes were measured from records lacking discrete events. Smooth curves are Gaussians with standard deviations 0.16 pA (*dark*) and 0.11 pA (*light*). Bandwidth 0–3 Hz.

neous rhodopsin activation has been removed by the procedure described above.

Separation of channel and continuous noise

To distinguish noise generated within the transduction cascade from noise arising from gating and/or blocking transitions in the cGMP-activated channels, noise spectra with synthesis and hydrolysis of cGMP disabled (see Materials and Methods and Fig. 1) were compared with spectra measured with the entire cascade functioning. Fig. 4 *A* shows noise spectra obtained from a truncated outer segment dialyzed with three different solutions: 1) ATP and GTP to keep the entire cascade working; 2) IBMX to inhibit cGMP hydrolysis and 0 GTP to prevent cGMP synthesis, with cGMP added to open channels and produce a current; and 3) the hydrolysis-resistant analog 8-bromo-cGMP to open channels and 0 GTP to prevent cGMP synthesis. Dark currents were 60 pA in solution 1), 130 pA in solution 2), and 140 pA in solution 3). Two components of noise are apparent in Fig. 4 *A*. One component extends to frequencies greater than 1 Hz, and the other component is dominated by frequencies less than 1 Hz.

The vertical scaling of the high frequency noise depended approximately linearly on the dark current, as shown in Fig. 4 *B*, where the difference spectra (dark − light) for each of the three conditions have been scaled by the corresponding dark currents to facilitate comparison. This scaling removed the differences in the high frequency noise in Fig. 4 *A*. We attribute the high frequency component to stochastic gating transitions in cGMP-activated channels and the low frequency component to cGMP concentration fluctuations generated within the phototransduction cascade (see below).

Disabling cGMP synthesis and hydrolysis had little effect on the high frequency noise, indicating that this component was not caused by cGMP concentration fluctuations generated within the cascade. Fig. 4 *C* shows difference spectra (dark − light) extended to 2 kHz with both cGMP synthesis

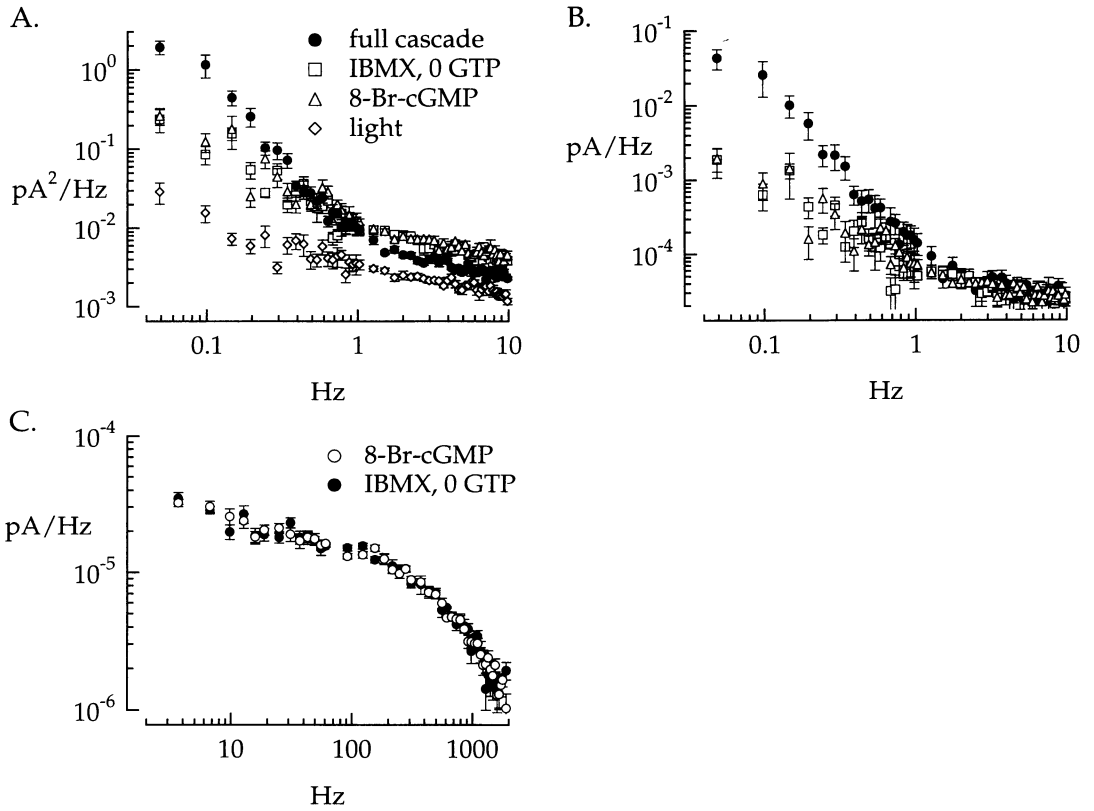

FIGURE 4 Separation of channel and continuous noise. (*A*) Spectra of a truncated outer segment's dark noise, measured as in Fig. 3, when it was dialyzed with one of three solutions: 1) standard internal solution with 1 mM GTP and 100 μM ATP to allow the entire cascade to function (●); 2) 0 GTP, 500 μM IBMX, and 27 μM cGMP to allow the dark current to flow in the absence of cGMP synthesis and hydrolysis (□); and 3) 0 GTP to prevent cGMP synthesis and 5 μM hydrolysis-resistant analog 8-bromo-cGMP to activate the channels (△). Instrumental noise measured in solution 1) during exposure to saturating light is also shown (◇). Dark current was 60 pA in solution 1), 130 pA in solution 2), and 140 pA in solution 3). Spectra (mean ± SEM) were computed from 15–25 records, each 20.48 s long, low-pass filtered at 20 Hz and digitized at 100 Hz; groups of four to eight records in each condition were interleaved. (*B*) Difference spectra (dark − light) in conditions 1–3 scaled vertically by the dark current. This scaling brought the noise at frequencies above 1 Hz into coincidence. (*C*) High-frequency component of noise in solutions 2) (●) and 3) (○), extended to 2 kHz. Spectra (mean ± SEM) computed from 25 records, each 1.6384 s long, low-pass filtered at 3 kHz and sampled at 10 kHz.

and hydrolysis disabled. Spectra were indistinguishable when the outer segment was dialyzed with cGMP and IBMX or with 8-bromo-cGMP. The rolloff at frequencies above 100 Hz was not due to stray capacitance in the recording apparatus, as the spectrum in saturating light was flat between 2 Hz and 2 kHz. Fig. 5 shows the power spectrum of the current fluctuations in a cell dialyzed with IBMX, 0 GTP, and cGMP over an extended frequency range; the smooth curve is the sum of four Lorentzians with half power frequencies of 0.1, 2.2, 80, and 1450 Hz. The half power frequencies and zero frequency asymptotes determined from seven such experiments are summarized in Table 2. Cyclic GMP channels in excised patches from toad rod outer segments (Matthews, 1986) generate noise fitted by a sum of two Lorentzians with half power frequencies similar to the two highest frequency components observed here. The additional low frequency components were apparent only when the power spectrum was measured at frequencies below 1 Hz; these additional components suggest that the cGMP-activated channel has long lived closed states.

When cGMP synthesis and hydrolysis were active, the dark noise at low frequencies (<1 Hz) increased substantially from the level set by channel noise (Fig. 4 *B*), indicating that this low-frequency component arose from cGMP concentration fluctuations generated by the cascade. This noise is the continuous component. The root-mean-square amplitude of the continuous noise was less than 0.2% of the dark current. Thus the continuous noise had only a small effect on the total number of open channels and the channel noise, and the channel and continuous noise should be nearly independent. The continuous component was isolated by computing the difference spectrum (noise with cascade functioning − noise with cascade disabled). This spectrum is shown in Fig. 5 *B* for the outer segment of Fig. 4. The smooth curve fitted to the spectrum was calculated according to Eq. 18, using the fitting procedure described in the Theory section.

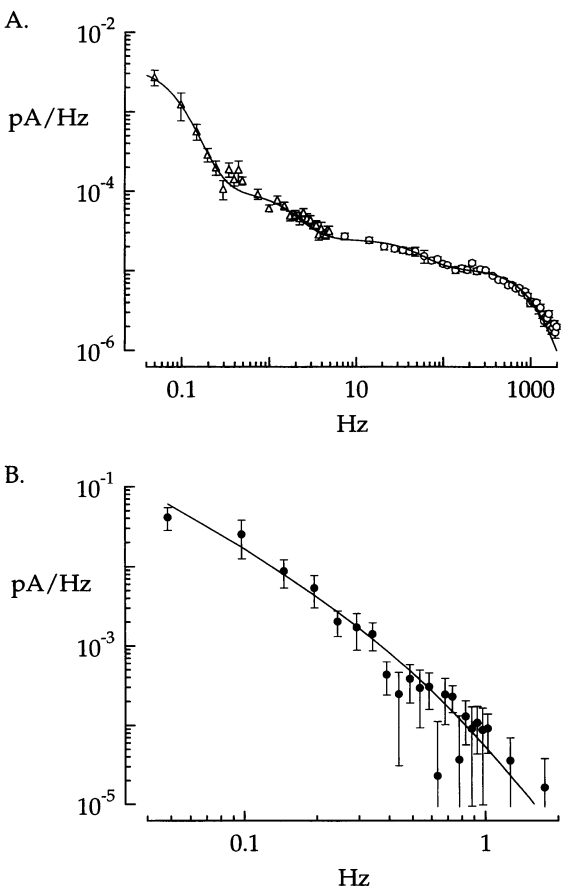

FIGURE 5 Channel and continuous noise spectra. (*A*) Difference spectra (dark − light) of membrane current fluctuations with cGMP synthesis and hydrolysis disabled. The truncated outer segment was dialyzed with a solution containing 0 GTP to disable cGMP synthesis and 500 μM IBMX to disable cGMP hydrolysis. Channels were activated by adding 27 μM cGMP to the dialysis solution. The spectrum has been normalized by the 70-pA dark current. The smooth curve is a sum of four Lorentzians with half-power frequencies of 0.1, 2.2, 80, and 1450 Hz and zero-frequency asymptotes of 3.5×10^{-3}, 7.0×10^{-5}, 1.4×10^{-5}, and 1.1×10^{-5} pA/Hz respectively. Bandwidth for measurement of noise 0–20 Hz for low-frequency spectrum (△) and 0–3000 Hz for high-frequency spectrum (○). (*B*) Continuous noise. Difference spectrum of noise generated within the cascade, calculated as (spectrum with entire cascade functioning, ● in Fig. 4 *B*) − (spectrum with synthesis and hydrolysis disabled, △ in Fig. 4 *B*). Smooth curve drawn according to Eq. 18 of text with $k_2 = 1.7\ s^{-1}$ and $\hat{a} = 2 \times 10^{-5}\ s^{-1}$ and scaled by the 60-pA dark current.

Source of continuous noise

Ca^{2+} fluctuations

The experiments described thus far indicate that the continuous noise is generated within the phototransduction cascade by cGMP concentration fluctuations. Before attempting to determine whether these fluctuations arise from fluctuations in the rate of cGMP synthesis or hydrolysis, we tested how dynamic changes in Ca^{2+} concentration influence the continuous noise. Because several elements of the transduction cascade are regulated by Ca^{2+} (reviewed by Koutalos and Yau, 1996), it seemed possible that fluctuations in the internal Ca^{2+} concentration might cause fluctuations in the rate of cGMP synthesis and/or hydrolysis. Alternatively, the rates of synthesis and/or hydrolysis might be subject to intrinsic fluctuations at constant Ca^{2+}.

A role of dynamic changes in Ca^{2+} was tested by measuring the dark noise in an intact rod with the internal Ca^{2+} clamped at the dark level or allowed to change normally (see Materials and Methods). As usual, the continuous component of the noise was isolated by selecting stretches of record lacking discrete events. If Ca^{2+} fluctuations caused or augmented the current fluctuations, less noise would be present with the internal Ca^{2+} clamped. Instead, the noise increased (Fig. 6 *A*). Clamping the internal Ca^{2+} also increased the amplitude and slowed the recovery of the dim flash response (Fig. 6 *B*), as reported previously (Matthews et al., 1988; Nakatani and Yau, 1988b). Upon clamping the Ca^{2+}, the variance of the continuous noise component increased by a factor of 5 ± 3, and the amplitude of the dim flash response increased by a factor of 2.6 ± 0.5 (four cells, mean ± SD). The increased amplitude of the noise and larger gain of the dim flash response are consistent with the known negative feedback between changes in intracellular Ca^{2+} and changes in current (reviewed by Koutalos and Yau, 1996).

A second test for a role of dynamic changes in Ca^{2+} in controlling the continuous noise was made by increasing the Ca^{2+} buffering capacity in the outer segment and thus slowing changes in Ca^{2+} (Rispoli et al., 1991). Current fluctuations in darkness were measured in an intact rod. Subsequently the rod was superfused with Ringer's plus 10 μM BAPTA-AM for 10–20 min, and the current fluctuations were remeasured. As reported by Rispoli et al. (1991), the amplitude of the continuous noise increased when the Ca^{2+} buffering capacity was increased (four cells, not shown). Results from both kinds of experiment—clamping internal Ca^{2+} and increasing the buffering capacity—indicate that Ca^{2+} changes damp the continuous noise.

Fluctuations in synthesis and hydrolysis

Experiments such as those in Figs. 4 and 6 indicate that the continuous noise is caused by fluctuations in the cGMP concentration independent of Ca^{2+} fluctuations. To test separately the role of fluctuations in hydrolysis and synthesis, a truncated outer segment was dialyzed with three different solutions: 1) GTP and ATP to allow the full cascade to function, 2) IBMX to inhibit cGMP hydrolysis and GTP to allow synthesis, and 3) IBMX and 0 GTP to disable both cGMP hydrolysis and synthesis and cGMP to open channels and produce a current. Dark noise spectra (dark − light) in each solution are shown in Fig. 7 *A*. Channel noise dominated each spectrum above 1 Hz. Assuming that the noise components arising from synthesis and hydrolysis are independent and additive, their separate contributions to the continuous noise were determined from difference spectra. The difference between the spectra measured in solutions 1) and 2) isolates the contribution to the noise of fluctuations in the rate of cGMP hydrolysis. The

TABLE 2 Parameters of channel noise

Component	Half-power frequency (Hz)		Zero-frequency asymptote (pA/Hz)	
	Mean	Range	Mean	Range
1	0.12 ± 0.04	0.10–0.18	$2.2 \pm 1.4 \times 10^{-3}$	$0.2–3.5 \times 10^{-4}$
2	1.6 ± 0.6	0.8–2.2	$8.9 \pm 6.9 \times 10^{-5}$	$0.2–1.8 \times 10^{-4}$
3	54 ± 37	24–86	$1.5 \pm 0.3 \times 10^{-5}$	$1.0–1.8 \times 10^{-5}$
4	860 ± 380	550–1450	$1.1 \pm 0.2 \times 10^{-5}$	$0.9–1.4 \times 10^{-5}$

Summary of parameters of the sum of four Lorentzians fitted to the power spectrum of current fluctuations with cGMP synthesis and hydrolysis disabled (Fig. 5 *A*). The table gives the mean (± SD) and range of the half-power frequencies and zero-frequency asymptotes of each component from seven outer segments dialyzed with 0 GTP, 500 nM IBMX, and 27 μM cGMP.

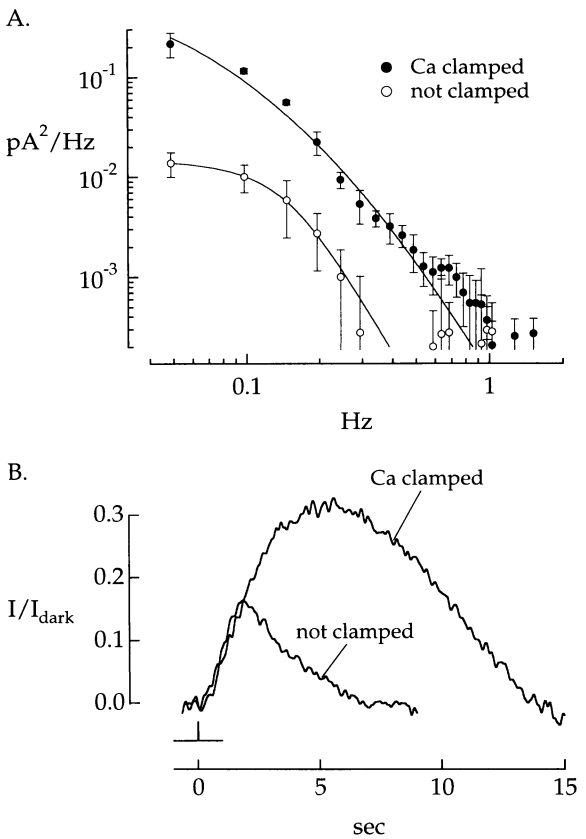

FIGURE 6 Effect of clamping the internal Ca^{2+} concentration on an intact rod's continuous noise spectrum and dim flash response. (*A*) Power spectra of the continuous noise with internal Ca^{2+} clamped (●) and allowed to change normally (○). The continuous noise spectrum was obtained by removing noise due to discrete events and instrumental noise (see Fig. 3). Spectra (mean ± SEM) calculated from 22 interleaved records, each 20.48 s long, low-pass filtered at 20 Hz and sampled at 100 Hz. The smooth curve fitted to the spectrum with the Ca^{2+} clamped is a product of two Lorentzians with rate constants of 0.05 and 0.16 Hz. The smooth curve fitted to the spectrum with Ca^{2+} allowed to change normally was calculated according to Eq. 26 with $\hat{a} = 1.4 \times 10^{-5}\ s^{-1}$ and $k_2 = 0.6\ s^{-1}$. (*B*) Averaged dim flash response with internal Ca^{2+} changing freely or clamped at the dark level by the technique described in Materials and Methods. The response amplitude has been normalized by the dark current, which was 8 pA (*clamped*) and 14 pA (*unclamped*). Flash delivered 9×10^{-2} photons μm^{-2} at 500 nm.

difference between the spectra measured in solutions 2) and 3) isolates the contribution of fluctuations in the rate of cGMP synthesis. Fig. 7 *B* compares these spectra with the noise generated by the full cascade (difference spectrum between solutions 1) and 3)). In nine such experiments, hydrolysis fluctuations alone accounted for 87 ± 4 % (mean ± SD) of the total current variance between 0 and 1 Hz. These results indicate that fluctuations in the rate of cGMP hydrolysis are the dominant source of the continuous noise.

Two further tests were made of the hypothesis that the continuous noise was caused by hydrolysis fluctuations. The first experiment tested whether IBMX suppressed the continuous noise in intact rods. The inner segment of an intact cell was drawn into a suction electrode so that the solution bathing the outer segment could be changed quickly. Noise spectra were measured with the internal Ca^{2+} concentration clamped (see Materials and Methods), so that the internal Ca^{2+} did not increase substantially when hydrolysis was suppressed and the dark current increased. At constant Ca^{2+}, IBMX should slow the rate of cGMP hydrolysis but not change the rate of cGMP synthesis. In the experiment shown in Fig. 8, exposure to IBMX increased the dark current from 12 pA to 36 pA (Fig. 8 *A*), as expected for a higher steady-state cGMP concentration resulting from a decreased hydrolysis rate. Despite the increase in dark current, the continuous component of the dark noise decreased (Fig. 8 *B*). The remaining low-frequency noise was probably due to incomplete block of PDE activity by 125 μM IBMX. The noise decrease could not have resulted from the saturation of channel activation by cGMP, because the maximum cGMP-activated currents were many times larger than those observed here (see below). In each of five experiments, IBMX increased the dark current while decreasing the continuous noise or leaving it unchanged; when corrected for the change in dark current (see below), exposure to IBMX suppressed the continuous noise in each experiment. Thus inhibition of PDE activity by IBMX decreased the continuous noise in intact cells as well as truncated outer segments.

The second experiment tested the scaling of the continuous noise with changes in dark current. If the continuous noise results from fluctuations in the rate of cGMP hydrolysis, the difference spectrum should scale with the square of the dark current. The noise spectrum S_I depends on the average square of the current fluctuation δI—i.e., $S_I = \langle|\delta I|^2\rangle$, where $\langle\cdots\rangle$ denotes an average over many examples of δI. Provided the cGMP concentration is well below the

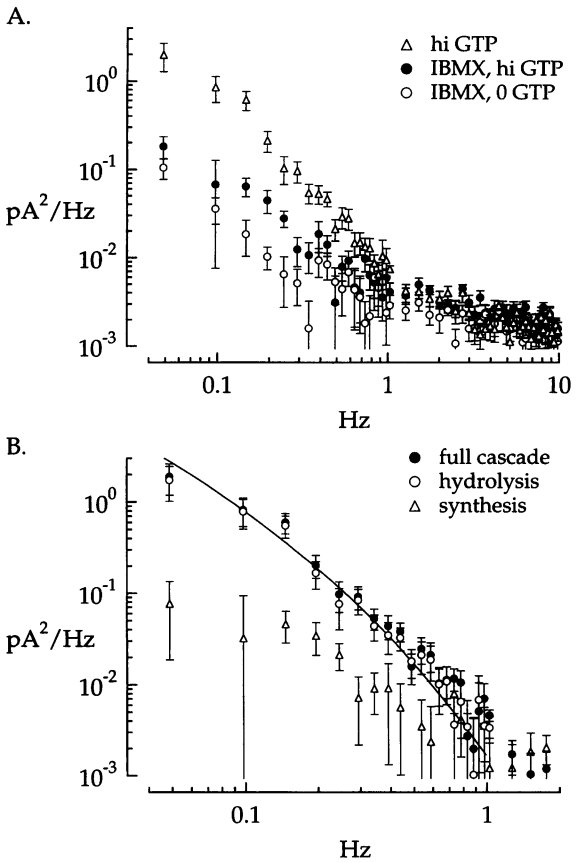

FIGURE 7 Evidence that fluctuations in the rate of cGMP hydrolysis made the principal contribution to the continuous noise. (*A*) Spectra of a truncated outer segment's dark noise, calculated from sweeps lacking discrete events. Spectra calculated from interleaved recordings with the outer segment dialyzed with one of three solutions: 1) 1 mM GTP, 100 μM ATP and 200 nM Ca^{2+}, allowing the entire cascade to operate (△); 2) 1 mM GTP, 100 μM ATP, 500 μM IBMX, and 400 nM free Ca^{2+}, allowing synthesis of cGMP but no hydrolysis (●), and 3) 0 GTP, 0 ATP, 500 μM IBMX and 27 μM cGMP to disable cGMP synthesis and hydrolysis yet permit channel activation (○). The concentrations of Ca^{2+} and cGMP in the three solutions were chosen to give similar dark currents. Instrumental noise measured in solution 1) after exposure to saturating light has been subtracted from each spectrum. Spectra (mean ± SEM) computed from 20–30 records in each condition. Bandwidth 0–20 Hz. (*B*) Separate contributions of cGMP synthesis and hydrolysis to the continuous dark noise. Spectrum of continuous dark noise was obtained as the difference between spectra in solutions 1) and 3) (●). Spectrum of contribution from hydrolysis alone was obtained as the difference between spectra in solutions 1) and 2) (○). Spectrum of the contribution from synthesis alone was obtained as the difference between spectra in solutions 2) and 3) (△). Dark currents were 65, 80, and 75 pA in solutions 1), 2), and 3), respectively. The smooth curve was calculated from Eq. 18 with $k_2 = 2.7\ s^{-1}$ and $\hat{a} = 1.7 \times 10^{-5}\ s^{-1}$ and scaled by the square of the dark current.

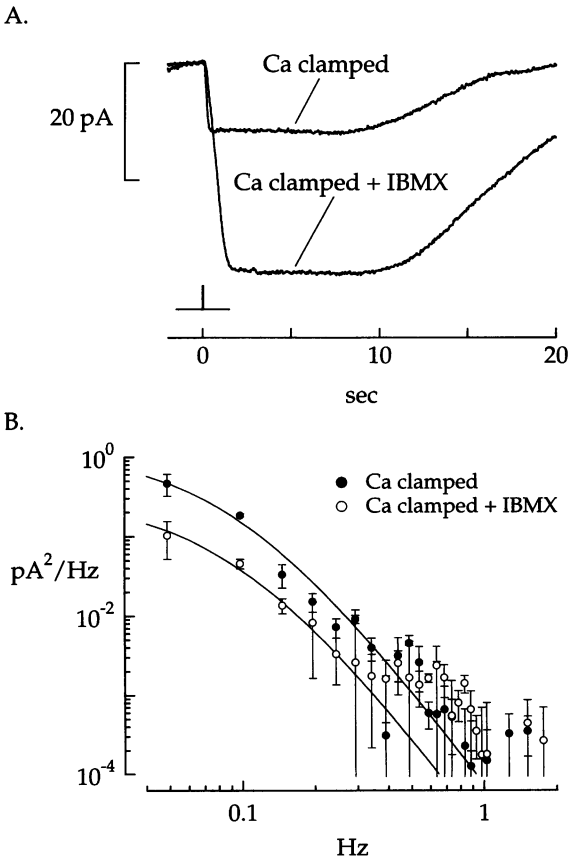

FIGURE 8 Inhibition of continuous noise by IBMX in an intact cell. Membrane current was recorded with the inner segment in the suction electrode and the outer segment's Ca^{2+} concentration clamped (see Materials and Methods). Records were taken with the normal Ca^{2+} clamp solution and with 125 μM IBMX added to the clamp solution. (*A*) Increase in dark current upon exposure to IBMX. Dark current was measured by exposure to a flash delivering 80 photons μm^{-2} at 500 nm. The light responses in the clamp solution are inverted because the external Na^+ was replaced with choline and the dark current was carried largely by outward movement of K^+. (*B*) Effect of IBMX on continuous noise. The cell was alternately exposed to the usual clamp solution (●) or to the clamp solution plus IBMX (○). The spectrum of current fluctuations in saturating light was subtracted from the spectra of dark fluctuations measured with and without IBMX. The continuous noise was isolated by analyzing only dark records lacking discrete events. Both smooth curves are a product of two Lorentzians with half-power frequencies 0.05 and 0.18 Hz. Spectra (mean ± SEM) computed from 12 records, each 20.48 s long. Bandwidth 0–20 Hz.

K_M of the PDE, a fluctuation δP in the PDE activity should produce a change in the cGMP concentration, G, proportional to $G\delta P$. The resulting change in current, δI, from Eq. 6 is $\delta I = 3\ hG^2\delta G \propto I\delta P$. Thus the spectrum S_I of the noise produced by fluctuations in the PDE activity should scale with the square of I. For other sources, the noise spectrum is likely to scale as a different power of the current. For example, noise generated by fluctuations in the rate of cGMP synthesis would scale as $I^{4/3}$ if individual cyclase molecules activate independently, the active state is improbable, and each activation produces a fixed number of cGMPs and thus a fixed change in current.

The experiment in Fig. 9 tested this prediction. Fig. 9 *A* shows difference spectra of the continuous noise (dark − light) from a truncated outer segment dialyzed with 36 μM cGMP, which gave a dark current of 22 pA, or 72 μM cGMP, which gave 75 pA. Although 72 μM cGMP is above the $K_{1/2}$ of the channels, the concentration of cGMP in most of the outer segment is considerably lower when hydrolysis

is proceeding normally. The noise spectra were scaled by I^n, and n was allowed to vary to bring the noise measured in low and high cGMP into correspondence. In the experiment of Fig. 9, the resulting value for n was 2.08 ± 0.13 (mean ± SD). Fig. 9 *B* compares the difference spectra measured in low and high cGMP scaled by the square of the corresponding dark currents. The mean value of n in a total of five experiments was 2.02 ± 0.08 (mean ± SEM); in these experiments the dark currents at 36 μM cGMP ranged from 20 to 50 pA, and the dark currents at 72 μM cGMP were 3–4 times larger. Thus the quantitative relation between the scaling of the noise spectrum and the square of the dark current is consistent with the notion that the noise resulted from spontaneous activation of PDE.

Lack of involvement of transducin

The experiments presented above demonstrate that fluctuations in the rate of cGMP hydrolysis constitute the major source of the continuous dark noise. These fluctuations might result from spontaneous activation of PDE itself or from spontaneous activation of transducin, which would in turn activate PDE. Normally transducin is activated by the binding of transducin-GDP to isomerized rhodopsin, which catalyzes the exchange of GDP for GTP. Transducin-GTP then activates PDE. Spontaneous activation of PDE might be triggered by spontaneous GDP-GTP exchange on transducin or perhaps by transducin-GDP itself.

To test for spontaneous GDP-GTP exchange on transducin in the absence of photoisomerized rhodopsin, a truncated outer segment was dialyzed initially with a solution containing cGMP and 10 μM GTP and subsequently with a solution containing cGMP but no GTP. Effective removal of GTP was indicated by a more than 1000-fold reduction in the flash sensitivity. Fig. 10 *A* shows that the continuous noise was not changed when GTP was removed. The dark current also did not change noticeably upon removal of GTP, further indicating that the mean dark PDE activity was largely independent of transducin activation. In six cells the ratio of the continuous noise variance with GTP to the variance without GTP was 1.1 ± 0.1 (mean ± SEM), and the dark current was unchanged upon removal of GTP. These results indicate that spontaneous GDP-GTP exchange on transducin did not contribute significantly to the spontaneous activation of PDE.

Biochemical experiments suggest that transducin-GDP may activate PDE at a low rate without GDP-GTP exchange (Kutuzov and Pfister, 1994). To test whether transducin-GDP participates in generation of the continuous noise, we observed the noise in a truncated outer segment dialyzed with a solution lacking GTP and ATP before and after bleaching the rhodopsin by exposure to a steady bright light. The bleaching exposure should cause all transducin to bind to rhodopsin, which in biochemical preparations renders transducin less able to activate PDE (Kutuzov and Pfister, 1994). This maneuver should decrease the noise if the

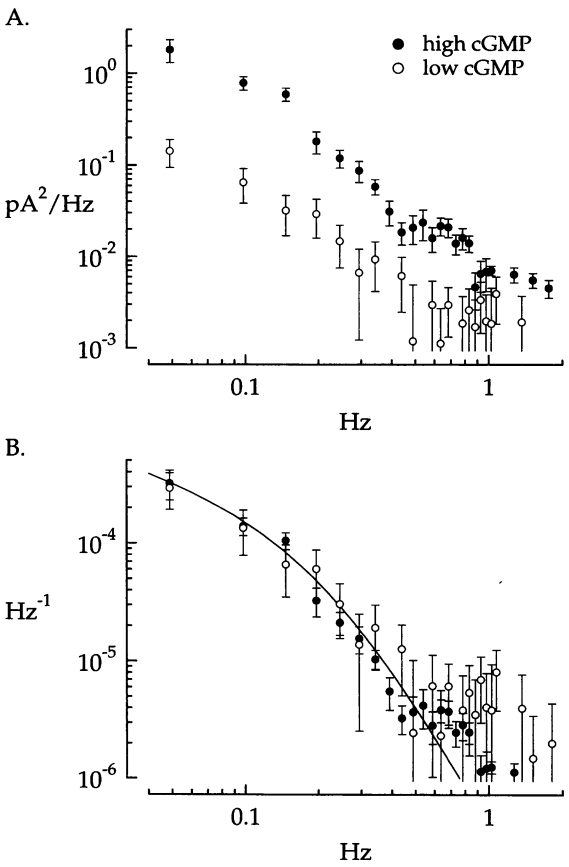

FIGURE 9 Scaling of continuous noise with square of dark current. The continuous component of dark noise was measured in a truncated outer segment dialyzed with 36 μM cGMP, which produced 22-pA dark current, or 72 μM cGMP, which produced 75-pA dark current. The solution dialyzing the outer segment contained 10 μM GTP and 1 mM ATP. (*A*) Difference spectra (dark − light) at 36 μM cGMP (○) and 72 μM cGMP (●). Spectra (mean ± SEM) computed from 20 records, each 20.48 s long. Bandwidth 0–20 Hz. (*B*) Difference spectra from *A* scaled by the square of the corresponding dark current. The smooth curve was calculated according to Eq. 15 with $k_2 = 1.5\ s^{-1}$ and $\hat{a} = 1.5 \times 10^{-5}\ s^{-1}$.

spontaneous PDE activity were triggered by transducin-GDP. Contrary to this prediction, exposure to bright light in the absence of GTP did not affect the continuous noise (Fig. 10 *B*). In four cells, the ratio of the variance between 0 and 1 Hz before and after exposure to saturating light was 1.2 ± 0.3 (mean ± SEM). Thus neither removal of GTP nor binding of transducin to rhodopsin eliminated the continuous noise. These observations indicate that the noise results from spontaneous activation of the PDE itself, without participation of transducin.

Mechanism of spontaneous PDE activation

It is well established that the γ subunits of PDE (hereafter referred to as gamma) inhibit the catalytic activity of the α and β subunits (reviewed by Yarfitz and Hurley, 1994). Transducin-GTP might activate PDE by completely removing gamma from the catalytic subunit or by causing it to

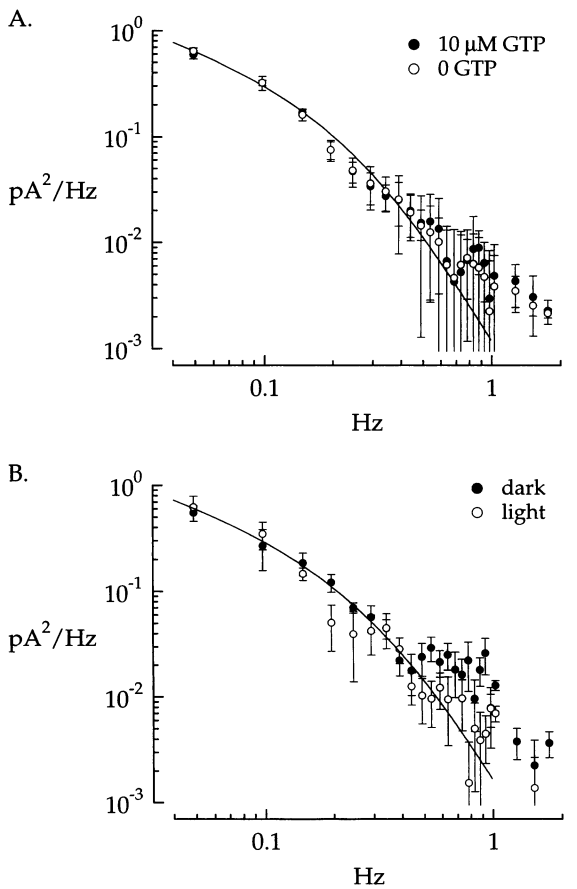

FIGURE 10 Lack of involvement of transducin in spontaneous PDE activity. (*A*) Difference spectra of continuous dark noise from a truncated outer segment dialyzed with 68 μM cGMP and 10 μM (●) or 0 GTP (○). Smooth curve drawn according to Eq. 15 with $k_2 = 1.9\ s^{-1}$ and $\hat{a} = 2.1 \times 10^{-5}\ s^{-1}$ scaled by the square of the dark current. Spectra (mean ± SEM) computed from 22 records, each 20.48 s long. Bandwidth 0–20 Hz. (*B*) Spectra of continuous noise measured before (●) and after (○) a truncated outer segment was exposed to a bleaching light expected to cause all transducin to bind to rhodopsin, as the dialyzing solution contained 0 GTP, 0 ATP, and 68 μM cGMP. The smooth curve was drawn according to Eq. 15 with $k_2 = 2.4\ s^{-1}$ and $\hat{a} = 1.6 \times 10^{-5}\ s^{-1}$ scaled by the square of the dark current. Spectra (mean ± SEM) were computed from 12 records, each 20.48 s long. Bandwidth 0–20 Hz.

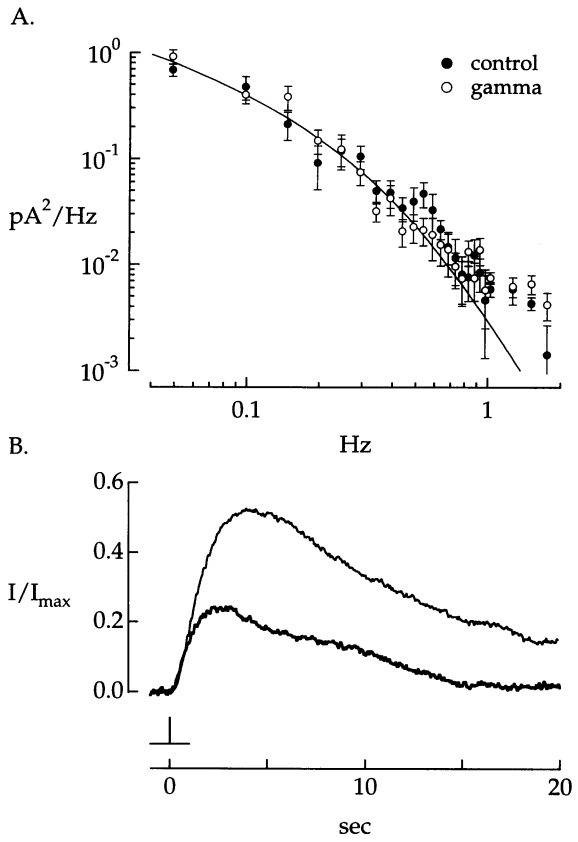

FIGURE 11 Lack of effect of exogenous PDE gamma on continuous noise. (*A*) Difference spectra (dark − light) were measured in a truncated outer segment dialyzed with (○) and without (●) 50 nM recombinant bovine gamma. The smooth curve was drawn according to Eq. 15 with $\hat{a} = 2.5 \times 10^{-5}\ s^{-1}$ and $k_2 = 2.5\ s^{-1}$ scaled by the square of the dark current. (*B*) Gamma reduced the amplitude of the dim-flash response. Responses to a flash delivering 7 photons μm^{-2} at 500 nm with and without 50 nM gamma.

move with respect to the catalytic subunit. If spontaneous activation of PDE involved complete dissociation of gamma from the catalytic subunit, the active PDE should become accessible to exogenous gamma, and the addition of gamma would be expected to decrease the continuous noise and increase the dark current. Recombinant bovine PDE gamma (Brown and Stryer, 1989) (kindly provided by Dr. Lane Brown) was introduced into a truncated outer segment at 50 or 500 nM. We estimate that the concentration of spontaneously active PDE is less than 10 nM (or 1 in 5000 PDEs; see Discussion), and thus the exogenous gamma in these experiments was present in concentrations 5–50 times larger than the concentration of active PDE. The addition of gamma did not affect the continuous noise (Fig. 11 *A*) or dark current. In six such experiments, the dark current did not change upon the addition of gamma, and the ratio of the current variances between 0 and 1 Hz with and without gamma was 0.9 ± 0.2 (mean ± SEM).

The sample of recombinant bovine gamma we used, however, did inhibit toad PDE. Trypsin-activated PDE was prepared from rod outer segments, and PDE activity was monitored by measuring the generation of protons by cGMP hydrolysis with the pH-sensitive dye SNAFL (Brown, 1992). Upon the addition of gamma, the pH quickly ceased to change, indicating that PDE activity was effectively inhibited. Furthermore, the addition of 50 nM recombinant gamma to the solution dialyzing the outer segment reversibly reduced the amplitude of the dim-flash response (Fig. 11 *B*). Exogenous gamma thus either inhibited light-activated (but not spontaneously activated) PDE or acted in the cascade at a site other than PDE. Although the mechanism of the effect on the flash response remains to be determined, the change shows that gamma effectively entered the outer segment and possessed biological activity.

The failure of exogenous gamma to inhibit spontaneous PDE activation indicates that the gamma binding site on

PDE was not accessible to exogenous gamma. Wensel and Stryer (1986) also found that exogenous gamma was unable to inhibit dark PDE activity completely. These results suggest that the γ subunit does not completely dissociate from the catalytic subunit during spontaneous activation. Instead, spontaneous PDE activation may occur when the γ subunit moves with respect to the catalytic subunit, thereby activating the catalytic site and allowing hydrolysis to proceed.

Hydrolytic activity and kinetics of single PDE molecules

Having identified the source of the continuous noise, it was possible to estimate the catalytic activity and activation/deactivation rate constants of a single PDE molecule, as described in the Theory section. Theoretical fits to the noise spectra depended on several quantities in addition to the catalytic activity $\hat{a}$ and activation/deactivation rate constants k_1 and k_2. For truncated outer segments the additional parameters were the cGMP diffusion coefficient D, the mean PDE activity P_D, and the dependence of the membrane current on cGMP concentration. For intact cells, the additional parameters were P_D, the Ca^{2+} exchange rate β, and the dependence of the current on cGMP concentration. These parameters were measured independently, as described in this section. Noise spectra were then fitted by Eqs. 15, 18, or 26 with $\hat{a}$ and k_2 as free parameters. The frequency of spontaneous PDE activation, Nk_1, was estimated from Eq. 2, and the rate constant k_1 for activation was estimated assuming that the total number of PDE molecules in the outer segment was $N = 3 \times 10^7$ (see Pugh and Lamb, 1993); N was not corrected for the small piece (~10%) of outer segment cut off during truncation.

Dependence of current on cGMP concentration

The relation between membrane current and cGMP concentration was measured by dialyzing a truncated outer segment with several concentrations of cGMP and normalizing the resulting steady-state currents by the current at saturating cGMP. IBMX was added to each dialyzing solution to inhibit cGMP hydrolysis. Fig. 12 *A* summarizes results from seven outer segments. The dependence of the membrane current I on the cGMP concentration G was fitted by the Hill equation (smooth curve):

$$\frac{I}{I_{max}} = \frac{1}{1 + (K_{1/2}/G)^n}, \qquad (27)$$

with $n = 2.9$ (see also Zimmerman and Baylor, 1986; Nakatani and Yau, 1988a; Koutalos et al., 1995a) and $K_{1/2} = 45$ μM. I_{max} in Eq. 27 is the current at saturating cGMP. For cGMP concentrations well below $K_{1/2}$, the current can be approximated as

$$I \approx hG^3, \qquad (28)$$

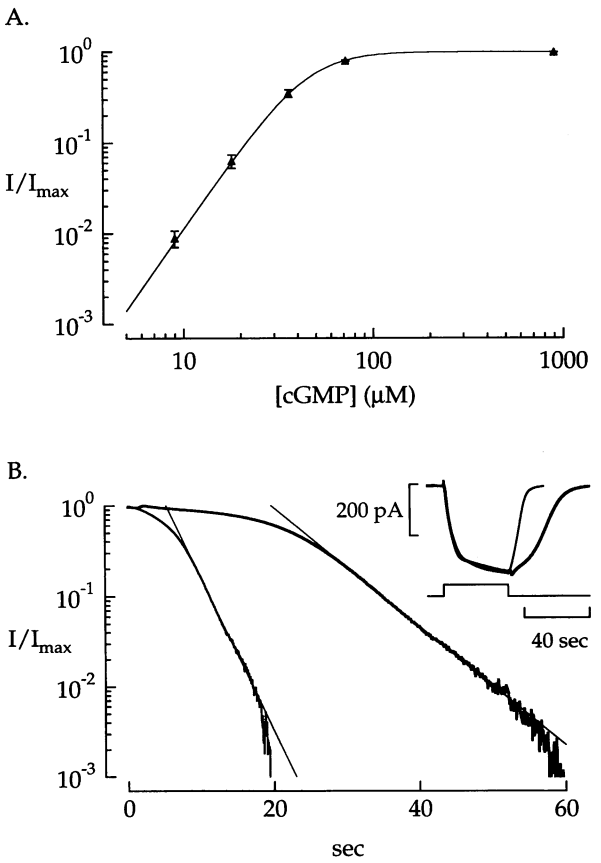

FIGURE 12 Parameters determining the shape of the continuous noise spectrum. (*A*) Dependence of steady-state outer-segment current on internal cGMP concentration in dialyzed, truncated outer segments. Cyclic GMP hydrolysis was suppressed with 500 μM IBMX. The cGMP-activated current, normalized by the maximum value, is plotted as a function of cGMP concentration on double logarithmic scales. The experimental points are mean values from measurements on seven outer segments; error bars are ±SEM. The smooth curve was drawn according to Eq. 27; the Hill coefficient n and $K_{1/2}$ from these results were $n = 2.9 \pm 0.1$ and $K_{1/2} = 45 \pm 4$ μM, the ranges giving 95% confidence intervals. Saturating currents ranged from 560 to 760 pA. (*B*) Determination of dark-adapted PDE activity and rate of longitudinal cGMP diffusion in a truncated outer segment. Normalized change in outer segment current is plotted on semilogarithmic axes as a function of time after the sudden removal of cGMP from the solution flowing over the cut end of the outer segment. The experiment was performed in the absence (*thin line*) and presence (*thick line*) of 500 μM IBMX to block cGMP hydrolysis. The inset shows a linear plot of the currents during application and removal of 180 μM cGMP. Current decays were fitted with exponentials (straight lines on the semilogarithmic plot) of rate constant 0.16 s^{-1} with IBMX and 0.41 s^{-1} without IBMX. The difference in the rate of decay, corrected for the nonlinear relation between cGMP concentration and current, yields the dark-adapted PDE activity (see Koutalos et al., 1995b, and text).

in which $h = I_{max}K_{1/2}^{-3} \approx 8 \times 10^{-3}$ pA μM^{-3}. The value for $K_{1/2}$ obtained in truncated outer segments (see also Koutalos et al., 1995a) is higher than that obtained in excised patches from rod outer segments (Zimmerman and Baylor, 1986; Haynes et al., 1986). The reason for the different behaviors of channels in intact outer segments and excised patches is not known.

Cyclic GMP diffusion coefficient and mean dark PDE activity

The effective longitudinal diffusion coefficient for cGMP and the mean dark PDE activity were estimated by analyzing the decline of membrane current upon removal of cGMP from the solution bathing the outer segment's cut end, with cGMP hydrolysis allowed to proceed or blocked (Koutalos et al., 1995b). The inset to Fig. 12 *B* shows the time course of the change in current that occurred when a truncated outer segment was exposed to 180 μM cGMP for 40 s in the presence (bold trace) or absence (thin trace) of IBMX. Fig. 12 *B* is a semilogarithmic plot of the decline in current upon removal of cGMP. After the current has fallen below half its maximum value, the cGMP concentration should decline exponentially, and the current should obey (Koutalos et al., 1995b)

$$\frac{I(t)}{I_{max}} = \exp\left(-3\left(P_D t + \frac{\pi^2 D t}{4L^2}\right)\right), \qquad (29)$$

where we have used the cubic relation between the current and the cGMP concentration (see Eq. 28). The final decline of the current in Fig. 12 *B* was indeed fitted by an exponential, with a rate constant of 0.16 s^{-1} without hydrolysis and 0.41 s^{-1} with hydrolysis. From the rate of decline without hydrolysis and the outer segment length of 50 μm, the diffusion coefficient was 55 $\mu m^2\ s^{-1}$. From the difference between the rate constants with and without hydrolysis, the dark PDE activity in this experiment was 0.08 s^{-1}. In similar experiments on six outer segments, the diffusion coefficient D was 57 ± 17 $\mu m^2\ s^{-1}$ (mean ± SD), and the dark PDE activity P_D was 0.10 ± 0.02 s^{-1}. Koutalos et al. (1995b) obtained cGMP diffusion coefficients between 50 and 70 $\mu m^2\ s^{-1}$ in salamander and frog rod outer segments. The value for P_D is two- to threefold lower than that obtained from experiments on salamander rods (Hodgkin and Nunn, 1988; Koutalos et al., 1995c).

Intracellular Ca^{2+} dynamics

The Na^+/K^+, Ca^{2+} exchange current was used to determine the kinetics of the fall in intracellular Ca^{2+} that followed a saturating flash (Nakatani and Yau, 1988c; Fig. 13). An intact rod was drawn into a suction electrode and exposed to a flash sufficiently bright to close all of the cGMP-activated channels for 10–15 s (Fig. 13 *A*, inset). The cGMP-activated channels closed quickly, leaving a small residual current due to Na^+/K^+, Ca^{2+} exchange (Nakatani and Yau, 1988c).

In agreement with recent studies (Rispoli et al., 1993; Gray-Keller and Detwiler, 1994; McCarthy et al., 1996), we found that a sum of two exponentials provided a better fit to the exchange current than a single exponential. Fig. 13 *B* is a semilogarithmic plot of the time course of the exchange current from Fig. 13 *A*. The smooth curve is a sum of two exponentials with rate constants of 2.5 and 0.41 s^{-1}. In a total of nine experiments, the mean rate constants and

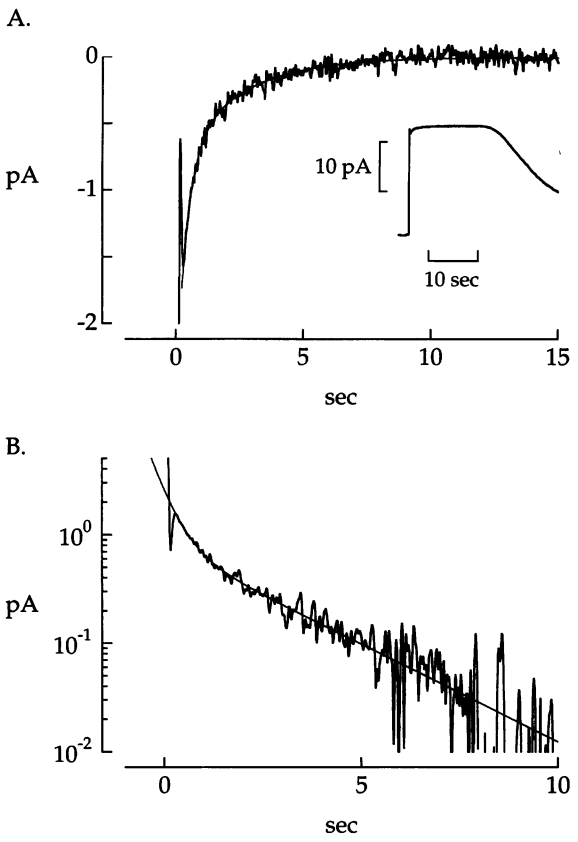

FIGURE 13 Na^+/K^+, Ca^{2+} exchange current kinetics. (*A*) Time course of exchange current after saturating flash. A flash delivering 6.1 × 10^3 photons μm^{-2} at 500 nm was delivered at time 0. In response to the flash the cGMP channels rapidly closed (entire response shown in *inset*); the remaining current is the Na^+/K^+, Ca^{2+} exchange current. The smooth curve is the two-exponential fit from *B* inverted and replotted on a linear scale. (*B*) Semilogarithmic plot of exchange current time course from *A*. The smooth curve fitted to the exchange current is a sum of two exponentials with rate constants of 0.41 and 2.5 s^{-1}.

amplitudes of the two exponential components were 1.9 ± 0.4 s^{-1} and 1.1 ± 0.5 pA for the fast component and 0.4 ± 0.2 s^{-1} and 0.5 ± 0.2 pA for the slow component (mean ± SD). The kinetics of Ca^{2+} changes in response to small, relatively fast changes in current, such as those generated by the continuous noise, are controlled largely by the fast component of the exchange current.

Estimation of PDE parameters k_1, k_2, and $\hat{a}$

The measured noise spectra in truncated outer segments were fitted using Eqs. 15 and 18, assuming D = 60 $\mu m^2\ s^{-1}$ and P_D = 0.1 s^{-1} while allowing the deactivation rate constant k_2 and catalytic activity $\hat{a}$ to vary. L was measured from stored video images and ranged from 30 to 50 μm. The measured noise spectra in intact cells were fitted using Eq. 26, assuming P_D = 0.1 s^{-1} and β = 2.0 s^{-1}. Table 3 summarizes the results of this analysis for intact cells and for truncated outer segments with and without cGMP synthesis; we estimate that the rate constant for spontaneous

TABLE 3 Kinetic parameters of PDE estimated from analysis of continuous noise spectra

Condition	#	$\hat{a}$ (s^{-1})	k_1 (s^{-1})	k_2 (s^{-1})
Intact cell	6	$1.8 \pm 0.6 \times 10^{-5}$	$3.5 \pm 2.8 \times 10^{-4}$	1.9 ± 1.5
Truncated with synthesis	11	$1.6 \pm 0.6 \times 10^{-5}$	$4.4 \pm 2.1 \times 10^{-4}$	2.1 ± 0.9
Truncated without synthesis	21	$1.5 \pm 0.8 \times 10^{-5}$	$3.5 \pm 2.4 \times 10^{-4}$	1.6 ± 0.6
Mean		$1.6 \pm 0.7 \times 10^{-5}$	$3.8 \pm 2.4 \times 10^{-4}$	1.8 ± 0.8

Fits of the continuous noise spectra by Eq. 15, 18, or 26 provided estimates of the rate constants for PDE activation, k_1, and deactivation, k_2, and the catalytic activity of a single PDE subunit, $\hat{a}$. The fits assumed a cGMP diffusion coefficient of $D = 60$ $\mu m\ s^{-1}$, a mean dark PDE activity of $P_D = 0.1\ s^{-1}$, a Ca^{2+} exchange rate of $\beta = 2.0\ s^{-1}$, and an outer segment length of $L = 30$–50 μm as measured from video images taken during the experiment. Entries are the mean ± SD from each type of experiment; the number of experiments of each type is given in the column labeled #.

PDE activation is $k_1 = 4 \pm 2 \times 10^{-4}\ s^{-1}$, the rate constant for PDE deactivation is $k_2 = 1.8 \pm 0.8\ s^{-1}$, and the catalytic activity of a single active PDE catalytic subunit is $\hat{a} = 1.6 \pm 0.7 \times 10^{-5}\ s^{-1}$.

DISCUSSION

The general conclusion from this work is that the continuous dark noise in the rod membrane current is produced by cGMP concentration fluctuations that result from spontaneous activation of PDE. Spontaneous activation appears to be an intrinsic property of the PDE molecule and does not involve transducin. Quantitative analysis of the noise provided estimates of the catalytic activity and activation-deactivation kinetics of single PDE molecules. These parameters add to an emerging quantitative picture of how amplification is achieved in the transduction cascade (reviewed by Pugh and Lamb, 1993). Spontaneous PDE activation matches the cGMP and Ca^{2+} turnover times, allowing rapid recovery of the flash response. Although spontaneous activation comes with a cost (an increase in dark noise), the magnitude of the noise is just small enough to leave photon detection unimpaired.

Gain in transduction

The estimated catalytic activity of a single active PDE subunit was $\hat{a} = 1.6 \times 10^{-5}\ s^{-1}$, and the estimated rate constant for PDE deactivation was $k_2 = 1.8\ s^{-1}$. The estimate of $\hat{a}$ is similar to that from biochemical measurements of the turnover rate and cGMP affinity of PDE (Dumke et al., 1994). A similar value of $\hat{a}$ allows quantitative description of the rising phase of the flash response (Pugh and Lamb, 1993). The similarity of the different estimates of $\hat{a}$ suggests that a PDE subunit that activates spontaneously has the full activity of one activated by transducin, and that transducin increases the rate constant k_1 for PDE activation.

Estimates of k_2 and $\hat{a}$ can be used to estimate the number of cGMP molecules hydrolyzed by a single active PDE and the number of PDEs activated by a single active rhodopsin. For a dark current of 20 pA, the internal cGMP concentration calculated from Eq. 28 is $G = 14$ μM. A single active PDE subunit hydrolyzes cGMPs at a rate of $\hat{a}G$, or about 2×10^{-4} $\mu M\ s^{-1}$. For an outer segment volume of 1 pl, this corresponds to hydrolysis of 120 cGMPs s^{-1}. Thus during its active lifetime of $1/k_2 \approx 0.5$ s, a single PDE subunit hydrolyzes about 60 cGMPs and produces a change in the cGMP concentration of about 10^{-4} μM. Longitudinal diffusion of cGMP causes the maximum local change to be less than 1 part in 10^3. From Eq. 6 a change in cGMP of 10^{-4} μM reduces the inward current by about 0.5 fA.

The single photon response in an intact toad rod has a peak amplitude of about 1 pA. Thus at the peak of the single photon response at least 2000 additional PDE molecules are active. This number is likely to be an underestimate. Local reduction in the cGMP concentration during the single photon response will cause the current change produced by a single active PDE to be less than 0.5 fA and thus increase the number of active PDEs required. Furthermore, the amplitude of the single photon response is reduced by Ca^{2+} feedback (Matthews et al., 1988; Nakatani and Yau, 1988b; Fig. 6). With the internal Ca^{2+} concentration clamped, the amplitude of the single photon response was observed to increase two- to threefold, which would require the activation of 4000–6000 PDEs at the response peak. This latter estimate of the rhodopsin-PDE gain will apply to the normal photon response if Ca^{2+} changes during the flash response act predominantly on the guanylate cyclase activity and do not alter the rhodopsin lifetime or the gain of the rhodopsin-transducin interaction. These considerations suggest that, at the response peak, a single active rhodopsin molecule activates at least 5000 additional PDEs.

The number of active PDEs created by a single active rhodopsin depends on both the rate of PDE activation by a single active rhodopsin and the rhodopsin lifetime. Because the efficiency of transducin-PDE coupling is thought to be close to 1 (see Pugh and Lamb, 1993), the rate of PDE activation is limited by the rate of transducin activation by rhodopsin. Light-scattering measurements provide an estimate of the rate of transducin activation of about 1000 s^{-1} (Vuong et al., 1984). An upper limit to the transducin activation rate is set by the rate of diffusional encounters between rhodopsin and transducin, which Pugh and Lamb (1993) calculate to occur at 7000 s^{-1}. Thus activation of 5000 PDEs requires that the rhodopsin lifetime be at least 700 ms, and likely longer than 1 s.

Spontaneous PDE activation and response kinetics

From the rate constant for spontaneous PDE activation, $k_1 \approx 4 \times 10^{-4}\ s^{-1}$, we estimate that a single PDE molecule

activates spontaneously about once every hour. The instability of the PDE molecule is enormous relative to that of rhodopsin, which activates spontaneously about once every 3000 years in a toad rod at room temperature (Baylor et al., 1980). The probability of finding a single PDE molecule active is k_1/k_2, so that about one PDE in 5000 is active at any given time.

The high rate of spontaneous PDE activation causes significant fluctuations in the rate of cGMP hydrolysis. As a result, a photoexcited rhodopsin molecule must activate enough PDEs to exceed the noise if reliable single photon detection is to occur. From this standpoint, spontaneous PDE activation seems to be an evil that the rod should avoid. Spontaneous PDE activation may, however, serve a useful role in adjusting the kinetics of the electrical response to light, as outlined below.

The effect of spontaneous PDE activation on the operation of the transduction cascade can be explored using the model described in the Theory section. Equations 24 and 25 describe the change in cGMP concentration that occurs in response to a brief pulse of PDE activity in an intact cell with Ca^{2+} feedback operating. The PDE pulse reduces the cGMP concentration, and the time required for cGMP to return to its dark level depends on the rate of cGMP synthesis. The synthesis rate in turn depends on two factors: the basal synthesis rate, which balances the basal hydrolysis rate P_D and determines the lifetime $1/P_D$ of a single cGMP molecule, and the Ca^{2+} turnover time $1/\beta$, which determines how quickly and how much the synthesis rate is increased during a change in current (see Eq. 20). The rate of spontaneous PDE activation determines P_D and thus the cGMP lifetime. Fig. 14 shows the calculated time course of the change in cGMP concentration produced by a brief pulse of PDE activity for several mean PDE activities. For

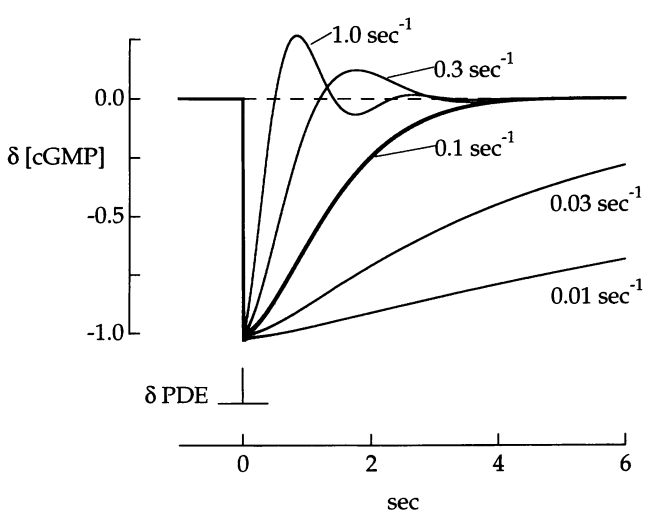

FIGURE 14 Effect of rate of spontaneous PDE activation on kinetics of cascade. The time course of the change in cGMP concentration produced by a brief pulse of PDE activity was calculated from Eqs. 24 and 25 with $\beta = 2\ s^{-1}$. Changes in cGMP concentration are plotted for mean PDE activities ranging from $0.01\ s^{-1}$ to $1\ s^{-1}$.

mean PDE activities greater than $0.1\ s^{-1}$, the impulse response is oscillatory because the lag in the Ca^{2+} feedback introduced by β causes the feedback to overcompensate the change in cGMP. For PDE activities less than $0.1\ s^{-1}$, the cGMP concentration returns to baseline very slowly because the mean dark cyclase rate is low. A mean PDE activity of $0.1\ s^{-1}$ quickly brings the cGMP concentration back to the dark level without an oscillation.

The measured mean PDE activity of $0.1\ s^{-1}$ produced by spontaneous PDE activation nicely matches the cGMP and Ca^{2+} turnover times, reaching a compromise between amplification and time resolution. Assuming spatial homogeneity, the predicted shape of the cGMP change in response to absorption of a single photon can be obtained by convolving one of the impulse responses in Fig. 14 with the time course of the PDE activity produced by an active rhodopsin. When $P_D > 0.1\ s^{-1}$, the effects of PDEs activated at different times during the light response would partially cancel each other, and amplification would suffer. When $P_D < 0.1\ s^{-1}$, the single-photon responses would be greatly prolonged and time resolution would suffer.

Implications for transducin and cyclase

No component of noise could be identified as arising from transducin. Thus there was no evidence for spontaneous GDP-GTP exchange on transducin or for PDE activation by transducin-GDP. Because transducin is present at a 10-fold higher concentration than PDE and a twofold increase in noise would have been obvious, the rate constant for spontaneous transducin activation is at least 20 times lower than the frequency of spontaneous PDE activation. We conclude that the rate constant for spontaneous transducin activation under physiological conditions is at most $2 \times 10^{-5}\ s^{-1}$. The rate of spontaneous GDP-GTP exchange measured biochemically has been estimated to be $10^{-4}\ s^{-1}$ (Ramdas et al., 1991), somewhat higher than the bounds set by our noise measurements.

A minor but consistently present component of noise could be identified with fluctuations in the rate of cGMP synthesis. The current variance associated with this component was approximately an order of magnitude smaller than that associated with hydrolysis fluctuations. Yet in steady state the mean rates of cGMP synthesis and hydrolysis must be equal. How does this occur? Assuming that individual enzyme molecules activate independently, that each active molecule has the same catalytic rate, and that the individual rates are additive, the mean and variance of the total catalytic rate are described by Poisson statistics. The mean rate is $\bar{x} = N_x \hat{a}_x$, and the variance is $\sigma_x^2 = N_x \hat{a}_x^2$, where N_x is the number of active molecules, and $\hat{a}_x$ is the catalytic rate of a single active molecule. The ratio of the ensemble variance to the mean depends only on the catalytic rate of a single molecule, $\sigma_x^2/\bar{x} = \hat{a}_x$. If cGMP synthesis and hydrolysis behave in accord with these assumptions, the equal mean rates but different contributions to the continuous noise

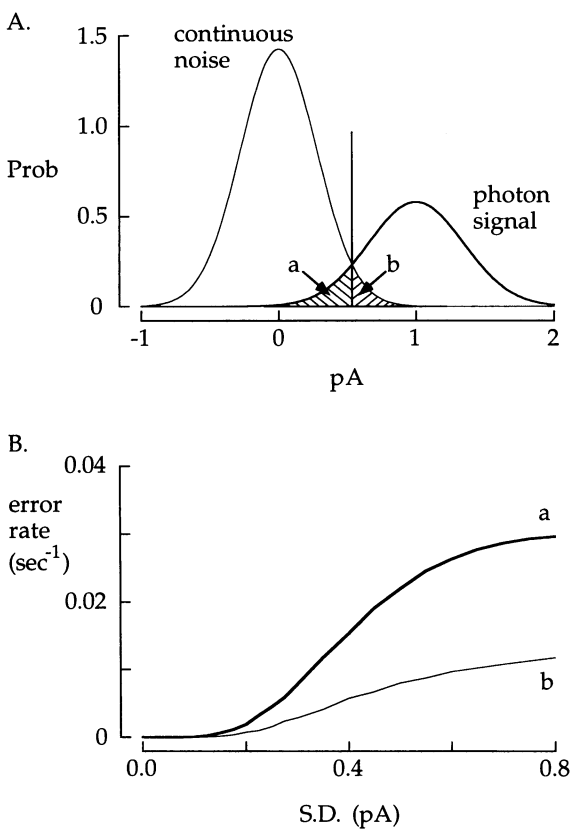

FIGURE 15 Continuous noise and single photon detection. (*A*) Schematic of amplitude distributions of noise and signal. The continuous noise generates false-positive single photon signals and causes some real events to go undetected. The distribution of current amplitudes generated by the continuous noise is well approximated by a Gaussian centered at 0 (see Fig. 3 *D*). The distribution of current amplitudes generated by effective single photon absorptions is also well approximated by a Gaussian, but with a nonzero mean amplitude. Discriminating single photon absorptions implies, given a response of amplitude *A*, deciding whether that response came from the continuous noise distribution or the photon-evoked signal distribution. For maximum likelihood discrimination, only response amplitudes to the right of the horizontal line are classified as photon absorptions. The area (*a*) under the photon signal distribution determines the number of real photon absorptions that go undetected because of the noise. The area (*b*) under the continuous noise distribution determines the number of false-positive responses generated by noise fluctuations. (*B*) False positives and missed responses as a function of the standard deviation of the continuous noise. Curves calculated for single photon response amplitude of 1 pA, standard deviation of single photon responses 0.2 pA, and light producing one effective isomerization every 30 s. The rate of missed responses was measured as the area in region *a* of part *A* divided by the total area of the photon signal distribution, multiplied by the rate of photon absorption. The rate of false-positive responses was measured as the area in region *b* of part *A* divided by the total area of the photon signal distribution multiplied by the rate of photon absorption.

variance imply that the synthesis rate of a single active cyclase is about an order of magnitude lower than the hydrolysis rate of a single active PDE. Each active PDE molecule hydrolyzes cGMP at a rate of about 120 s^{-1}, and in darkness a single active guanylate cyclase would synthesize cGMP at no more than 10–15 s^{-1}. Thus the small contribution of cyclase activity to the dark noise can be explained by the low catalytic rate of a single molecule.

Implications for single photon detection

The continuous noise may impair reliable photon detection in two ways. First, large noise fluctuations may be mistaken for single photon responses. Second, the noise may cause some single photon responses to go undetected. The importance of these effects can be gauged from the amplitude distributions of the single photon response and the continuous noise after filtering matched to the single photon response (Baylor et al., 1980); this filtering removes as much noise as possible while preserving the single photon signals. The amplitude distribution of single photon responses in toad rods is approximately Gaussian, with a mean near 1 pA and a standard deviation of 0.2 pA (Baylor et al., 1979b), whereas the amplitude distribution of the filtered continuous noise fluctuations is Gaussian, with a standard deviation about 0.2 pA (see Fig. 15 *A*). A simple way to discriminate signals from noise is maximum likelihood estimation. We choose a threshold where the dark noise distribution and the single photon response distribution are equal and assume that when the current exceeds threshold, a photon response has occurred (Fig. 15 *A*). The frequency of false-positive responses is the area under the noise curve above threshold; the frequency of missed responses is the area under the response curve below threshold. These two types of error are plotted in Fig. 15 *B* as a function of the standard deviation of the noise. A standard deviation of 0.2 pA for the continuous noise would produce false photon-like events at a rate of about 1 per 1000 s, well below the rate of thermal activation of rhodopsin. At this noise level about 5% of single photon responses would go undetected. If the rms amplitude of the noise were twice as large, the rate of false-positive responses would increase to about 1 per 100 s, and more than 20% of the true responses would go undetected. Thus regulation of the total number of PDE molecules in the outer segment and their frequency of activation are crucial for reliable single photon detection.

We thank Drs. R. L. Brown, E. J. Chichilnisky, M. Feller, M. Meister, W. G. Owen, L. Stryer, and T. Wensel for careful reading of the manuscript; Robert Schneevies for excellent technical assistance; and Dr. R. L. Brown for helpful discussions, a supply of recombinant PDE gamma, and help with the assay of PDE activity.

This work was supported by National Eye Institute grants EY01543 (to DAB) and EY06456 (to FR).

REFERENCES

Aho, A.-C., K. Donner, C. Hydèn, L. O. Larsen, and T. Reuter. 1988. Low retinal noise in animals with low body temperature allows high visual sensitivity. *Nature.* 324:348–350.

Aho, A.-C., K. Donner, and T. Reuter. 1993. Retinal origins of the temperature effect on absolute visual sensitivity in frogs. *J. Physiol. (Lond.).* 463:501–521.

Barlow, H. B. 1956. Retinal noise and absolute threshold. *J. Opt. Soc. Am.* 46:634–639.

Barlow, H. B., W. R. Levick, and M. Yoon. 1971. Responses to single quanta of light in retinal ganglion cells of the cat. *Vision Res.* 11:87–102.

Baylor, D. A., T. D. Lamb, and K.-W. Yau. 1979a. The membrane current of single rod outer segments. *J. Physiol. (Lond.).* 288:589–611.

Baylor, D. A., T. D. Lamb, and K.-W. Yau. 1979b. Responses of retinal rods to single photons. *J. Physiol. (Lond.).* 288:613–634.

Baylor, D. A., G. Matthews, and K.-W. Yau. 1980. Two components of electrical dark noise in toad retinal rod outer segments. *J. Physiol. (Lond.).* 309:591–621.

Baylor, D. A., and B. J. Nunn. 1986. Electrical properties of the light-sensitive conductance of rods of the salamander *Ambystoma tigrinum*. *J. Physiol. (Lond.).* 371:115–145.

Baylor, D. A., B. J. Nunn, and J. L. Schnapf. 1984. The photocurrent, noise and spectral sensitivity of rods of the monkey *Macaca fascicularis*. *J. Physiol. (Lond.).* 357:575–607.

Bodoia, R. D., and P. B. Detwiler. 1984. Patch-clamp recordings of the light-sensitive dark noise in retinal rods from the lizard and frog. *J. Physiol. (Lond.).* 367:183–216.

Brown, R. L. 1992. Functional regions of the inhibitory subunit of rod cGMP phosphodiesterase identified by site specific mutagenesis and fluorescence spectroscopy. *Biochemistry.* 31:5918–5925.

Brown, R. L., and L. Stryer. 1989. Expression in bacteria of functional inhibitory subunit of retinal rod cGMP phosphodiesterase. *Proc. Natl. Acad. Sci. USA.* 86:4922–4926.

Carslaw, H. S., and J. C. Jaeger. 1959. Conduction of Heat in Solids, 2nd Ed. Clarendon Press, Oxford, England.

Cervetto, L., L. Lagnado, R. J. Perry, D. W. Robinson, and P. A. McNaughton. 1989. Extrusion of calcium from rod outer segments is driven by both sodium and potassium gradients. *Nature.* 337:740–743.

Colquhoun, D., and A. G. Hawkes. 1977. Relaxation and fluctuations of membrane currents that flow through drug-operated channels. *Proc. R. Soc. Lond. B.* 199:231–262.

Copenhagen, D. R., K. Donner, and T. Reuter. 1987. Ganglion cell performance at absolute threshold in toad retina: effects of dark events in rods. *J. Physiol. (Lond.).* 393:667–680.

Dumke, C. H., V. Y. Arshavsky, P. D. Calvert, M. D. Bownds, and E. N. Pugh. 1994. Rod outer segment structure influences the apparent kinetic parameters of cyclic GMP phosphodiesterase. *J. Gen. Physiol.* 103: 1071–1098.

Gray, P., and D. Attwell. 1985. Kinetics of light-sensitive channels in vertebrate photoreceptors. *Proc. R. Soc. Lond. B.* 223:379–388.

Gray-Keller, M. P., and P. B. Detwiler. 1994. The calcium feedback signal in the phototransduction cascade of vertebrate rods. *Neuron.* 13: 849–861.

Haynes, L. W., A. R. Kay, and K.-W. Yau. 1986. Single cyclic GMP-activated channel activity in excised patches of rod outer segment membrane. *Nature.* 321:66–70.

Hecht, S., S. Shlaer, and M. Pirenne. 1942. Energy, quanta and vision. *J. Gen. Physiol.* 25:819–840.

Hodgkin, A. L., and B. J. Nunn. 1988. Control of the light sensitive current in salamander rods. *J. Physiol. (Lond.).* 403:439–471.

Koch, K. W., and L. Stryer. 1988. Highly cooperative feedback control of retinal rod guanylate cyclase by calcium ions. *Nature.* 334:64–66.

Koutalos, Y., K. Nakatani, T. Tamura, and K.-W. Yau. 1995a. Characterization of guanylate cyclase activity in single retinal rod outer segments. *J. Gen. Physiol.* 106:863–890.

Koutalos, Y., K. Nakatani, and K.-W. Yau. 1995b. Cyclic GMP diffusion coefficient in rod photoreceptor outer segments. *Biophys. J.* 68:373–382.

Koutalos, Y., K. Nakatani, and K.-W. Yau. 1995c. The cGMP-phosphodiesterase and its contribution to sensitivity regulation in retinal rods. *J. Gen. Physiol.* 106:891–921.

Koutalos, Y., and K.-W. Yau. 1996. Regulation of sensitivity in vertebrate rod photoreceptors by calcium. *Trends Neurosci.* 19:73–81.

Kutuzov, M., and C. Pfister. 1994. Activation of the retinal cGMP-specific phosphodiesterase by the GDP-loaded alpha-subunit of transducin. *Eur. J. Biochem.* 220:963–971.

Lagnado, L., and D. A. Baylor. 1992. Signal flow in visual transduction. *Neuron.* 8:995–1002.

Lagnado, L., and D. A. Baylor. 1994. Calcium controls light-triggered formation of catalytically active rhodopsin. *Nature.* 367:273–277.

Lamb, T. D. 1987. Sources of noise in photoreceptor transduction. *J. Opt. Soc. Am. A.* 4:2295–2300.

Leibrock, C. S., T. Reuter, and T. D. Lamb. 1994. Dark adaptation of toad rod photoreceptors following small bleaches. *Vision Res.* 34:2787–2800.

Matthews, G. 1986. Comparison of the light-sensitive and cyclic GMP-sensitive conductances of the rod photoreceptor: noise characteristics. *J. Neurosci.* 6:2521–2526.

Matthews, H. R., R. L. W. Murphy, G. L. Fain, and T. D. Lamb. 1988. Photoreceptor light adaptation is mediated by cytoplasmic calcium concentration. *Nature.* 334:67–69.

McCarthy, S. T., J. P. Younger, and W. G. Owen. 1994. Free calcium concentrations in bullfrog rods determined in the presence of multiple forms of Fura-2. *Biophys. J.* 67:2076–2089.

McCarthy, S. T., J. P. Younger, and W. G. Owen. 1996. Dynamic spatially non-uniform calcium regulation in frog rods exposed to light. *J. Neurophysiol.* In press.

Nakatani, K., and K.-W. Yau. 1988a. Guanosine 3′,5′-cyclic monophosphate-activated conductance studied in a truncated rod outer segment of the toad. *J. Physiol. (Lond.).* 395:731–753.

Nakatani, K., and K.-W. Yau. 1988b. Calcium and light adaptation in retinal rods and cones. *Nature.* 334:69–71.

Nakatani, K., and K.-W. Yau. 1988c. Calcium and magnesium fluxes across the plasma membrane of the toad rod outer segment. *J. Physiol. (Lond.).* 395:695–729.

Pugh, E. N., Jr., and T. D. Lamb. 1993. Amplification and kinetics of the activation steps in phototransduction. *Biochem. Biophys. Acta.* 1141: 111–149.

Ramdas, L., R. M. Disher, and T. G. Wensel. 1991. Nucleotide exchange and cGMP phosphodiesterase activation by pertussis toxin inactivated transducin. *Biochemistry.* 30:11637–11645.

Rice, S. O. 1954. Mathematical analysis of random noise. *In* Noise and Stochastic Processes. N. Wax, editor. Dover, New York.

Rispoli, G., W. A. Sather, and P. B. Detwiler. 1991. Ca regulation of the guanylate cyclase is responsible for low frequency light-sensitive noise in retinal rods. *Biophys. J.* 59:534a.

Rispoli, G., W. A. Sather, and P. B. Detwiler. 1993. Visual transduction in dialysed detached rod outer segment from lizard retina. *J. Physiol. (Lond.).* 465:513–537.

Sakitt, B. 1972. Counting every quantum. *J. Physiol. (Lond.).* 223: 131–150.

Vuong, T. M., M. Chabre, and L. Stryer. 1984. Millisecond activation of transducin in the cyclic nucleotide cascade of vision. *Nature.* 311: 659–661.

Wensel, T. G., and L. Stryer. 1986. Reciprocal control of retinal rod cyclic GMP phosphodiesterase by its γ subunit and transducin. *Proteins.* 1:90–99.

Yarfitz, S., and J. B. Hurley. 1994. Transduction mechanisms of vertebrate and invertebrate photoreceptors. *J. Biol. Chem.* 269:14329–14332.

Yau, K.-W., and K. Nakatani. 1985. Light-suppressible, cyclic GMP-sensitive conductance in the plasma membrane of a truncated rod outer segment. *Nature.* 317:252–255.

Zimmerman, A. L., and D. A. Baylor. 1986. Cyclic GMP-sensitive conductance of retinal rods consists of aqueous pores. *Nature.* 321:70–72.

Zimmerman, A. L., G. Yamanaka, F. Eckstein, D. A. Baylor, and L. Stryer. 1985. Interaction of hydrolysis-resistant analogs of cyclic GMP with the phosphodiesterase and light-sensitive channel of retinal rod outer segments. *Proc. Natl. Acad. Sci. USA.* 82:8813–8817.